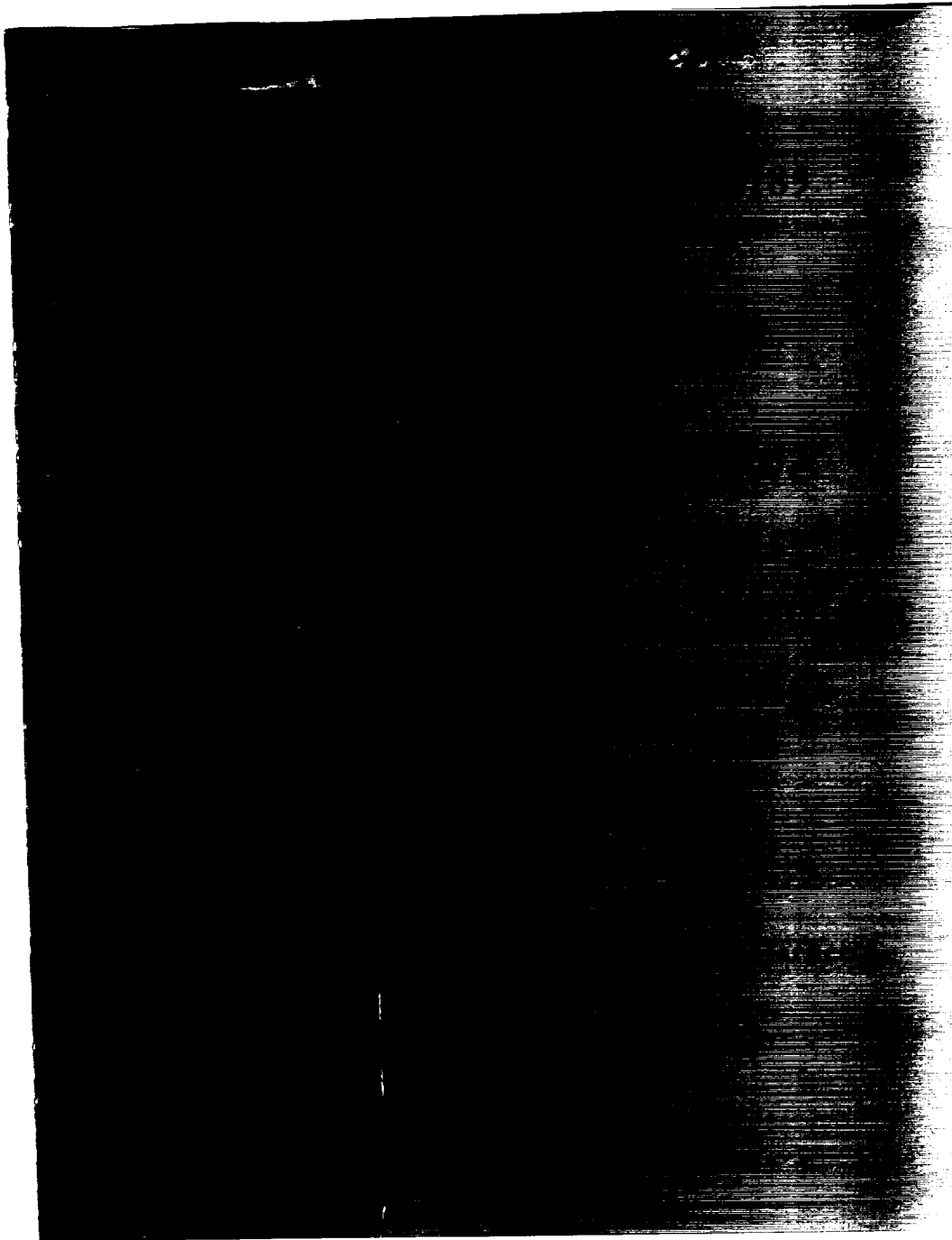

(NASA-CR-4185) A TRANSONIC INTERACTIVE BOUNDARY-LAYER THEORY FOR LAMINAR AND TURBULENT FLOW OVER SWEPT WINGS Final Report (North Carolina State Univ.) 82 p CSCL 01A

N89-10029

Unclas
H1/02 0166293

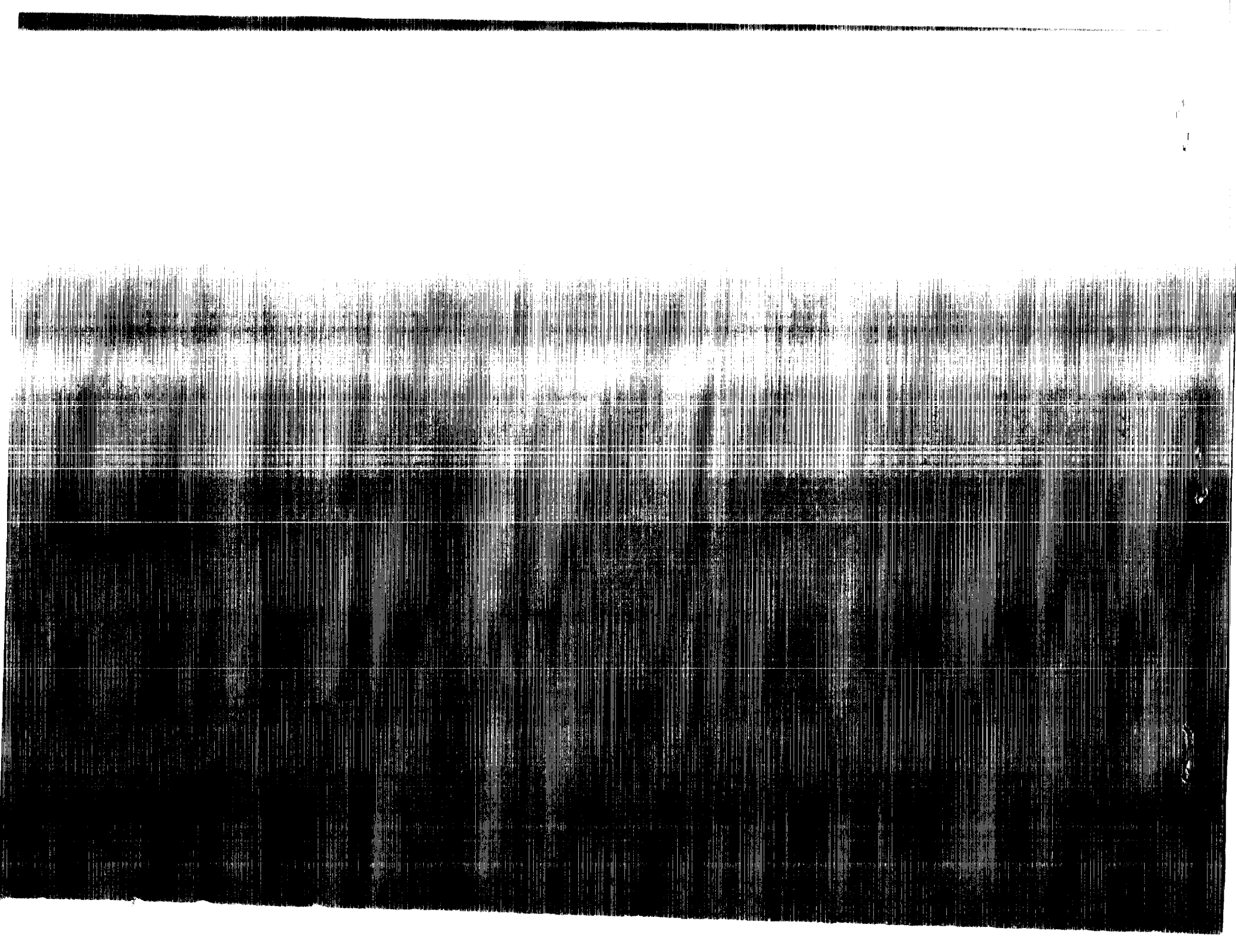

NASA Contractor Report 4185

A Transonic Interactive Boundary-Layer Theory for Laminar and Turbulent Flow Over Swept Wings

Shawn H. Woodson and Fred R. DeJarnette
North Carolina State University
Raleigh, North Carolina

Prepared for
Langley Research Center
under Cooperative Agreement NCC1-22

National Aeronautics
and Space Administration

Scientific and Technical
Information Division

1988

SUMMARY

A three-dimensional laminar and turbulent boundary-layer method is developed for compressible flow over swept wings. The governing equations and curvature terms are derived in detail for a nonorthogonal, curvilinear coordinate system. Reynolds shear-stress terms are modeled by the Cebeci-Smith eddy-viscosity formulation. The governing equations are descritized using the second-order accurate, predictor-corrector finite-difference technique of Matsuno, which has the advantage that the crossflow difference formulas are formed independent of the sign of the crossflow velocity component.

The method is coupled with a full potential wing-body inviscid code (FLO-30) and the inviscid-viscous interaction is performed by updating the original wing surface with the viscous displacement surface calculated by the boundary-layer code. The number of these "global" iterations ranged from five to twelve depending on the Mach number, sweep angle, and angle of attack. Several test cases are computed by this method and the results are compared with another inviscid-viscous interaction method (TAWFIVE) and with experimental data.

ACKNOWLEDGEMENTS

The authors would like to express their sincere gratitude to the people of the Advanced Configurations Branch of the NASA Langley Research Center for supporting this work through cooperative agreement NCC1-22. A special note of thanks to the technical monitor, Dr. James F. Campbell, for his continuous encouragement and advice during the course of this research, which served as the basis for the first author's Ph.D. dissertation. Also, we are deeply indebted to Mrs. Anne Cary for her excellent work in the preparation of this manuscript.

TABLE OF CONTENTS

SYMBOLS

a_e-d_e	coefficients in eq. (78)
a_m-e_m	coefficients in eq. (77)
a_s, b_s, c_s	parameters in eq. (B12)
A	parameter defined by eq. (8b)
AR	aspect ratio
b, c_1, c_2	parameters defined by eq. (32)
c	chord length, $\bar{x}_{te} - \bar{x}_{le}$
C_{f_s}, C_{f_y}	skin-friction coefficients, eqs. (80), (81)
C_f	local skin-friction coefficient, eq. (91)
C_p	pressure coefficient, $C_p = 2(p - p_\infty)/\rho_\infty u_\infty^2$
$d\ell$	differential line element, eqs. (B40), (B41)
$\frac{D}{Dt}$	substantial derivative, eq. (B18)
$\hat{e}_s, \hat{e}_y, \hat{e}_n$	curvilinear unit vectors
E	total enthalpy profile, eq. (32)
$\bar{f}$	parameter defining wing cross-sections
f, g	parameters defined by eqs. (25), (26)
$\bar{F}$	parameter defining wing surface, eq. (A4)
F, G	velocity profiles, eqs. (27), (28)
g_{ij}	fundamental tensor, eq. (B42)
h_1, h_2	metric coefficients, eqs. (A20), (A21)
h	static enthalpy
H	total enthalpy, $H = h + u_T^2/2$
$\hat{i}, \hat{j}, \hat{k}$	Cartesian unit vectors
K_1, K_2	geodesic curvatures, eqs. (B21), (B22)
K_{12}, K_{21}	parameters defined by eqs. (B24), (B25)

L	parameter defined by eq. (8a)
m_1-m_{12}	coefficients defined by eq. (33)
p	pressure
p_s, p_y, p_n	parameters in eq. (B26)
Pr	Prandtl number, $Pr = 0.72$
Pr_t	turbulent Prandtl number, $Pr_t = 0.90$
q	dummy argument, eq. (B12)
$\vec{R}$	position vector, eq. (A15)
Re	local Reynolds number, $Re = u_e s/\nu_e$
s,y,n	nonorthogonal curvilinear coordinates
t_1-t_{17}	coefficients defined by eqs. (C4), (C8)
T	temperature
u,v,w	curvilinear velocity components
$\bar{u},\bar{v},\bar{w}$	Cartesian velocity components
u_{ref}	constant reference velocity
u_T	magnitude of total velocity, eq. (B35)
u_s, v_y	$\frac{\partial u}{\partial s_r}$, $\frac{\partial v}{\partial y_{le}}$
u_∞	freestream velocity
$\vec{V}$	velocity vector, eq. (B1)
V^i	contravariant velocity vector, eq. (B45)
$\bar{x},\bar{y},\bar{z}$	Cartesian (orthogonal) coordinates
Y	fraction of semispan
β_e	inviscid yaw-plane inclination angle, eq. (92)
β_w	limiting streamline angle, eq. (82)
β_1- β_8	parameters defined by eq. (35)
γ_1- γ_5	parameters defined by eq. (59)

Γ	angle defined by eq. (A7)
$\Gamma_1 - \Gamma_4$	vectors defined by eq. (39)
δ_{ij}	Kronecker delta
δ_η, δ_y	central difference operators, eqs. (63), (64)
δ_s^*, δ_y^*	velocity integral thicknesses, eqs. (84), (85)
Δ	angle defined by eq. (A3)
Δ_η, Δ_s	central difference operators, eqs. (65), (66)
Δ^*	three-dimensional displacement surface, eq. (86)
∇	vector gradient operator, eq. (A5)
∇_s	backward difference operator, eq. (68)
ε_m	eddy-viscosity coefficient, eq. (7)
ζ, Z	vectors defined by eq. (36)
η	transformed normal coordinate, eqs. (23), (49)
θ	angle between s- and y-coordinate lines
κ	wing cross-section angle
λ	taper ratio
Λ	wing sweep angle, eq. (A2)
μ	dynamic viscosity coefficient
ν	kinematic viscosity coefficient
ξ	constant chord line, eq. (A1)
ρ	density
$-\rho\overline{u'w'}$, $-\rho\overline{v'w'}$, $-\rho\overline{w'H'}$	Reynolds stresses, eq. (6)
$\sigma_1 - \sigma_5$	coefficients defined by eq. (34)
τ_s, τ_y	$\mu \frac{\partial u}{\partial n}, \mu \frac{\partial v}{\partial n}$
τ_{ij}	stress tensor, eq. (B36)

ϕ,ψ	stream functions, eqs. (24), (44), (52)
Ω	angle defined by eq. (A13)

Subscripts

e	edge of the boundary layer
i	inner
i,j,k	mesh point location, eq. (62)
le	leading edge
o	outer
r	root chord
te	trailing edge
T	total
w	wall
0	$\overline{z}$ = 0 plane
∞	freestream conditions

INTRODUCTION

To obtain accurate flow field calculations over wings and wing-body combinations, the effects of viscosity must be accounted for in the solution. This may be accomplished by either solving some form of the Navier-Stokes equations or by interacting an inviscid code with a viscous boundary-layer method. The solution of the three-dimensional Navier-Stokes equations requires extremely large computer storage in order to resolve the various length scales and thus, also requires very long calculation run times. Therefore a great deal of attention has been focused on the more economical inviscid-viscous interaction procedure.

The interaction is performed by updating the inviscid solution by either a displacement surface or transpiration velocity component calculated by the boundary-layer code and then rerunning the inviscid code. This procedure is repeated until successive viscous updates are less than some specified tolerance. The methods of Streett [1] and McLean and Randall [2] interact a full potential inviscid code with a three-dimensional boundary-layer method by use of the displacement surface. A code in which the interaction is performed by the transpiration velocity component was developed by Wai, et al. [3]. Each of these methods requires the solution of some form of the three-dimensional boundary-layer equations.

Streett [1] and Wai [3] chose to solve the boundary-layer equations in the integral form, where the governing partial differential equations have been integrated in the normal direction. Swafford and Whitfield [4] developed a time-dependent integral method for the three-dimensional boundary-layer equations but did not perform the inviscid-viscous interaction. A drawback of the integral approach is that one must choose, a priori, the shape of the velocity profiles. For example, in Streett's method the crossflow velocity profile cannot predict a crossflow profile with velocity crossover, a situation which occurs quite often for three-dimensional flows. Also, integral methods are generally less flexible than differential methods.

The method of McLean and Randall [2] solves the boundary-layer equations in the differential form for a body-oriented curvilinear coordinate system. However, the coordinate system they used is orthogonal with one surface coordinate along the constant chord lines and the other perpendicular to them. This type of coordinate system requires a large clustering of grid points in the trailing edge region to resolve the outboard portion of a swept and tapered wing. Further, the wing root- and tip-chord lines do not lie along grid lines so the solution may not be determined along these lines. The use of a nonorthogonal coordinate system alleviates these problems.

Viscous methods which solve the three-dimensional boundary-layer equations in a nonorthogonal coordinate system have been developed by Cebeci, et al. [5], Matsuno [6], and Van Dalsem and Steger [7]. However, none of these methods were interacted with an inviscid code. In this paper, a three-dimensional laminar and turbulent boundary-layer method is developed for compressible flow over arbitrary swept wings and coupled to a full potential inviscid code through a displacement surface calculation. The inviscid solution procedure used to drive the boundary-layer method is the FLO-30 code

developed by Caughey and Jameson [8] which solves the full-potential equation in a conservative, finite-volume form for flow over wing-fuselage combinations. The wake is treated as a contact discontinuity across which the pressure is continuous but the tangential velocity component is discontinuous. This inviscid code was also employed by Streett [1,9] to interact with an integral boundary-layer method to develop a code called TAWFIVE and further details of the procedure are provided in references 8 and 9.

For the present method, viscous effects are only determined on the wing. The inviscid-viscous interaction is performed by running the inviscid code and using the inviscid velocity distribution to drive the boundary-layer code. The viscous displacement surface calculated by the boundary-layer code is added to the original wing surface and the inviscid solution is then determined for the new wing surface (wing plus displacement thickness). The displacement surface updates are slightly under-relaxed to minimize oscillations. The number of these "global" iterations varied from about five to twelve depending on the Mach number, sweep angle, and angle of attack.

GOVERNING BOUNDARY-LAYER EQUATIONS

The nonorthogonal curvilinear coordinate system is illustrated in figures 1 and 2 and the unit vectors and metric coeffifients for this body-oriented system are derived in Appendix A. The independent surface variables are s_r and y_{le} where s_r refers to s measured along the root-chord line and y_{le} refers to y measured along the wing leading edge. The angle θ is the angle between the s- and y-coordinate lines. The three-dimensional laminar and turbulent boundary-layer equations are derived in detail for this coordinate system in Appendix B. For convenience, they are simply listed here as:

continuity equation,

$$\frac{\partial}{\partial s_r}(\rho u h_2 \sin\theta) + \frac{\partial}{\partial y_{le}}(\rho v h_1 \sin\theta) + \frac{\partial}{\partial n}(\overline{\rho w}\, h_1 h_2 \sin\theta) = 0 \tag{1}$$

streamwise momentum equation,

$$\frac{\rho u}{h_1}\frac{\partial u}{\partial s_r} + \frac{\rho v}{h_2}\frac{\partial u}{\partial y_{le}} + \overline{\rho w}\frac{\partial u}{\partial n} - \rho K_1 \cot\theta\, u^2 + \rho K_2 \csc\theta\, v^2$$

$$+ \rho K_{12}\, uv = \rho_e \left[\frac{u_e}{h_1}\frac{\partial u_e}{\partial s_r} + \frac{v_e}{h_2}\frac{\partial u_e}{\partial y_{le}} - K_1 \cot\theta\, u_e^2\right.$$

$$\left. + K_2 \csc\theta\, v_e^2 + K_{12}\, u_e\, v_e\right] + \frac{\partial}{\partial n}\left(\mu\frac{\partial u}{\partial n} - \rho\,\overline{u'w'}\right) \tag{2}$$

spanwise momentum equation,

$$\frac{\rho u}{h_1}\frac{\partial v}{\partial s_r} + \frac{\rho v}{h_2}\frac{\partial v}{\partial y_{1e}} + \overline{\rho w}\frac{\partial v}{\partial n} - \rho K_2 \cot\Theta\, v^2 + \rho K_1 \csc\Theta\, u^2$$

$$+ \rho K_{21} uv = \rho_e \left[\frac{u_e}{h_1}\frac{\partial v_e}{\partial s_r} + \frac{v_e}{h_2}\frac{\partial v_e}{\partial y_{1e}} - K_2 \cot\Theta\, v_e^2\right.$$

$$\left. + K_1 \csc\Theta\, u_e^2 + K_{21} u_e v_e\right] + \frac{\partial}{\partial n}\left(\mu\frac{\partial v}{\partial n} - \rho\overline{v'w'}\right) \tag{3}$$

energy equation,

$$\frac{\rho u}{h_1}\frac{\partial H}{\partial s_r} + \frac{\rho v}{h_2}\frac{\partial H}{\partial y_{1e}} + \overline{\rho w}\frac{\partial H}{\partial n}$$

$$= \frac{\partial}{\partial n}\left[\frac{\mu}{Pr}\frac{\partial H}{\partial n} + \mu\left(1 - \frac{1}{Pr}\right)\frac{\partial}{\partial n}\left(\frac{u_T^2}{2}\right) - \rho\overline{w'H'}\right] \tag{4}$$

where h_1 and h_2 are the metric coefficients, K_1 and K_2 are the geodesic curvatures of the curves y_{1e} = constant and s_r = constant, respectively, and K_{12} and K_{21} are geometric parameters which are functions of the metric coefficients and geodesic curvatures. Their explicit values are provided in the Appendices.

The boundary conditions on the above equations are:

$$n = 0 \quad , \quad u = v = w = 0 \quad , \quad \left(\frac{\partial H}{\partial n}\right)_w = 0 \quad \text{or} \quad T = T_w$$

$$n = \infty \quad , \quad u = u_e \quad , \quad v = v_e \quad , \quad H = H_e \tag{5}$$

In order to close the system of equations, some assumptions for the Reynolds stresses must be made. For the present study, the Cebeci-Smith [10] eddy-viscosity model is employed. This relates the turbulent stresses to the mean velocity and total enthalpy profiles by,

$$-\rho\overline{u'w'} = \rho\,\varepsilon_m\frac{\partial u}{\partial n} \quad , \quad -\rho\overline{v'w'} = \rho\,\varepsilon_m\frac{\partial v}{\partial n} \tag{6a}$$

$$-\rho\overline{w'H'} = \rho\frac{\varepsilon_m}{Pr_t}\frac{\partial H}{\partial n} \tag{6b}$$

where Pr_t is the turbulent Prandtl number and the eddy-viscosity coefficient is defined in the inner layer by [5],

$$(\varepsilon_m)_i = L^2 \left[\left(\frac{\partial u}{\partial n}\right)^2 + \left(\frac{\partial v}{\partial n}\right)^2 + 2\cos\theta \left(\frac{\partial u}{\partial n}\right)\left(\frac{\partial v}{\partial n}\right)\right]^{1/2} \tag{7a}$$

and in the outer layer by [5],

$$(\varepsilon_m)_o = 0.0168 \left| \int_0^\infty (u_{Te} - u_T)\, dn \right| \tag{7b}$$

where,

$$L = 0.4\, n \left[1 - e^{-(n/A)}\right] \tag{8a}$$

$$A = 26\, \nu \left(\frac{\rho}{\tau_{Tw}}\right)^{1/2} \tag{8b}$$

$$\tau_{Tw} = \mu_w \left[\left(\frac{\partial u}{\partial n}\right)_w^2 + \left(\frac{\partial v}{\partial n}\right)_w^2 + 2\cos\theta \left(\frac{\partial u}{\partial n}\right)_w \left(\frac{\partial v}{\partial n}\right)_w\right]^{1/2} \tag{8c}$$

In order to solve eqs. (1)-(4) an inviscid solution has to be provided, either by an inviscid code or experiment, and both initial and side boundary conditions must be determined since the equations are of the parabolic type. The initial conditions will be the flow along the attachment line of the wing and the side boundaries will be the flow along the root- and tip-chord lines. For the flow along the wing tip an infinite swept wing assumption is made whereby the flow variables are assumed to be independent of the spanwise coordinate. Therefore, along the wing tip the governing equations reduce to:

continuity equation,

$$\frac{\partial}{\partial s_r}(\rho u h_2 \sin\theta) + \frac{\partial}{\partial n}(\overline{\rho w}\, h_1 h_2 \sin\theta) = 0 \tag{9}$$

streamwise momentum equation,

$$\frac{\rho u}{h_1}\frac{\partial u}{\partial s_r} + \overline{\rho w}\frac{\partial u}{\partial n} - \rho K_1 \cot\theta\, u^2 + \rho K_2 \csc\theta\, v^2 + \rho K_{12}\, uv$$

$$= \rho_e\left[\frac{u_e}{h_1}\frac{\partial u_e}{\partial s_r} - K_1 \cot\theta\, u_e^2 + K_2 \csc\theta\, v_e^2 + K_{12} u_e v_e\right]$$

$$+ \frac{\partial}{\partial n}\left(\mu\frac{\partial u}{\partial n} - \rho\overline{u'w'}\right) \tag{10}$$

spanwise momentum equation,

$$\frac{\rho u}{h_1}\frac{\partial v}{\partial s_r} + \overline{\rho w}\frac{\partial v}{\partial n} - \rho K_2 \cot\Theta\, v^2 + \rho K_1 \csc\Theta\, u^2 + K_{21} uv$$

$$= \rho_e\left[\frac{u_e}{h_1}\frac{\partial v_e}{\partial s_r} - K_2 \cot\Theta\, v_e^2 + K_1 \csc\Theta\, u_e^2 + K_{21}\, u_e v_e\right]$$

$$+ \frac{\partial}{\partial n}\left(\mu\frac{\partial v}{\partial n} - \rho\overline{v'w'}\right) \tag{11}$$

energy equation,

$$\frac{\rho u}{h_1}\frac{\partial H}{\partial s_r} + \overline{\rho w}\frac{\partial H}{\partial n} = \frac{\partial}{\partial n}\left[\frac{\mu}{Pr}\frac{\partial H}{\partial n} + \mu\left(1 - \frac{1}{Pr}\right)\frac{\partial}{\partial n}\left(\frac{u_T^2}{2}\right) - \rho\overline{w'H'}\right] \tag{12}$$

The boundary conditions for the infinite-swept-wing equations are the same as those given for the general equations.

The root chord line of the wing is assumed to be a line of symmetry where the spanwise derivatives of all the flow variables except v are zero. Along this line $v = 0$, and to the boundary-layer approximation, the spanwise momentum equation is singular. However, differentiating the spanwise momentum equation with respect to y_{le} yields a nonsingular equation. Therefore, along the root-chord line the governing equations become:

continuity equation,

$$\frac{\partial}{\partial s_r}(\rho u h_2 \sin\Theta) + \rho\, h_1 \sin\Theta\, v_y + \frac{\partial}{\partial n}(\overline{\rho w}\, h_1 h_2 \sin\Theta) = 0 \tag{13}$$

streamwise momentum equation,

$$\frac{\rho u}{h_1}\frac{\partial u}{\partial s_r} + \overline{\rho w}\frac{\partial u}{\partial n} - \rho\, K_1 \cot\Theta\, u^2 = \rho_e\left[\frac{u_e}{h_1}\frac{\partial u_e}{\partial s_r} - K_1 \cot\Theta\, u_e^2\right]$$

$$+ \frac{\partial}{\partial n}\left(\mu\frac{\partial u}{\partial n} - \rho\,\overline{u'w'}\right) \tag{14}$$

spanwise momentum equation,

$$\frac{\rho u}{h_1}\frac{\partial v_y}{\partial s_r} + \frac{\rho v_y^2}{h_2} + \overline{\rho w}\frac{\partial v_y}{\partial n} + \rho u^2 \frac{\partial}{\partial y_{le}}(K_1 \csc\Theta) + \rho\, K_{21}\, u\, v_y$$

$$= \rho_e \left[\frac{u_e}{h_1}\frac{\partial v_{ye}}{\partial s_r} + \frac{v_{ye}^2}{h_2} + u_e^2 \frac{\partial}{\partial y_{1e}}(K_1 \csc\Theta) + K_{21}\, u_e\, v_{ye}\right]$$

$$+ \frac{\partial}{\partial n}\left[\mu \frac{\partial v_y}{\partial n} - \rho\,(\overline{v'w'})_y\right] \tag{15}$$

energy equation,

$$\frac{\rho u}{h_1}\frac{\partial H}{\partial s_r} + \overline{\rho w}\frac{\partial H}{\partial n} = \frac{\partial}{\partial n}\left[\frac{\mu}{Pr}\frac{\partial H}{\partial n} + \mu\left(1 - \frac{1}{Pr}\right)\frac{\partial}{\partial n}\left(\frac{u^2}{2}\right) - \rho\,\overline{w'H'}\right] \tag{16}$$

where v_y means the derivative of v with respect to y_{1e}. The boundary conditions for the above equations are:

$$n = 0 \quad , \; u = v_y = w = 0 \quad , \quad \left(\frac{\partial H}{\partial n}\right)_w = 0$$

$$n = \infty \quad , \quad u = u_e \quad , \; v_y = v_{ye} \quad , \quad H = H_e \tag{17}$$

The initial conditions are obtained by applying eqs. (1)-(4) along the attachment line of the wing. However, along the attachment line, $u = 0$, and to the boundary-layer approximation, the streamwise momentum equation is singular. It is therefore necessary to differentiate it with respect to s_r to obtain a nonsingular equation. Thus, along the attachment line the governing equations become:

continuity equation,

$$\rho h_2 \sin\Theta\, u_s + \frac{\partial}{\partial y_{1e}}(\rho v h_1 \sin\Theta) + \frac{\partial}{\partial n}(\overline{\rho w}\, h_1 h_2 \sin\Theta) = 0 \tag{18}$$

streamwise momentum equation,

$$\frac{\rho u_s^2}{h_1} + \frac{\rho v}{h_2}\frac{\partial u_s}{\partial y_{1e}} + \overline{\rho w}\frac{\partial u_s}{\partial n} + \rho v^2 \frac{\partial}{\partial s_r}(K_2 \csc\Theta) + \rho\, K_{12}\, u_s\, v$$

$$= \rho_e\left[\frac{u_{se}^2}{h_1} + \frac{v_e}{h_2}\frac{\partial u_{se}}{\partial y_{1e}} + v_e^2 \frac{\partial}{\partial s_r}(K_2 \csc\Theta) + K_{12}\, u_{se}\, v_e\right]$$

$$+ \frac{\partial}{\partial n}\left[\mu \frac{\partial u_s}{\partial n} - \rho\,(\overline{u'w'})_s\right] \tag{19}$$

spanwise momentum equation,

$$\frac{\rho v}{h_2}\frac{\partial v}{\partial y_{le}} + \overline{\rho w}\frac{\partial v}{\partial n} - \rho K_2 \cot\Theta\, v^2 = \rho_e\left[\frac{v_e}{h_2}\frac{\partial v_e}{\partial y_{le}} - K_2 \cot\Theta\, v_e^2\right]$$

$$+ \frac{\partial}{\partial n}\left[\mu\frac{\partial v}{\partial n} - \rho\,\overline{v'w'}\right] \qquad (20)$$

energy equation,

$$\frac{\rho v}{h_2}\frac{\partial H}{\partial y_{le}} + \overline{\rho w}\frac{\partial H}{\partial n} = \frac{\partial}{\partial n}\left[\frac{\mu}{Pr}\frac{\partial H}{\partial n} + \mu\left(1 - \frac{1}{Pr}\right)\frac{\partial}{\partial n}\left(\frac{v^2}{2}\right) - \rho\,\overline{w'H'}\right] \qquad (21)$$

where u_s means the derivative of u with respect to s_r. The boundary conditions for the attachment-line equations are:

$$n = 0 \quad , \quad u_s = v = w = 0 \quad , \quad \left(\frac{\partial H}{\partial n}\right)_w = 0$$

$$n = \infty \quad , \; u_s = u_{se} \quad , \; v = v_e \quad , \quad H = H_e \qquad (22)$$

TRANSFORMATION OF THE GOVERNING EQUATIONS

Before proceeding to descritize the governing three-dimensional boundary-layer equations, it is convenient to introduce a non-dimensional parameter which scales the growth of the boundary layer. A variable η is defined by the transformation,

$$\eta = \left(\frac{u_e}{\nu_e s}\right)^{1/2}\int_0^n \frac{\rho}{\rho_e}\,dn \quad , \quad s = \int_0^{s_r} h_1\,ds_r \qquad (23)$$

Two stream functions are also defined by,

$$\rho u h_2 \sin\Theta = \frac{\partial\psi}{\partial n} \; , \; \rho v h_1 \sin\Theta = \frac{\partial\phi}{\partial n} \; ,$$

$$\overline{\rho w}\, h_1 h_2 \sin\Theta = -\left(\frac{\partial\psi}{\partial s_r} + \frac{\partial\phi}{\partial y_{le}}\right) \qquad (24)$$

which automatically satisfies the continuity equation. In addition, the parameters $f(s_r, y_{le}, \eta)$ and $g(s_r, y_{le}, \eta)$ are defined by the relations,

$$\psi = (\rho_e \mu_e u_e s)^{1/2} h_2 \sin\Theta f \tag{25}$$

$$\phi = \left(\frac{\rho_e \mu_e s}{u_e}\right)^{1/2} u_{ref} h_1 \sin\Theta g \tag{26}$$

where u_{ref} is a constant (usually chosen as the freestream velocity, u_∞). Using eqs. (23), (25), and (26) in eq. (24) yields,

$$\frac{u}{u_e} = \frac{\partial f}{\partial \eta} = F(s_r, y_{le}, \eta) \tag{27}$$

$$\frac{v}{u_{ref}} = \frac{\partial g}{\partial \eta} = G(s_r, y_{le}, \eta) \tag{28}$$

With eqs. (23)-(28), the governing three-dimensional boundary-layer equations become:

streamwise momentum equation,

$$\frac{\partial}{\partial \eta}\left[b \frac{\partial F}{\partial \eta}\right] + \sigma_2 \frac{\partial F}{\partial \eta} + m_7 \left(\frac{\partial g}{\partial y_{le}} \frac{\partial F}{\partial \eta} - G \frac{\partial F}{\partial y_{le}}\right)$$

$$+ m_{10} \left(\frac{\partial f}{\partial s_r} \frac{\partial F}{\partial \eta} - F \frac{\partial F}{\partial s_r}\right) = m_2 F^2 + m_5 FG + m_8 G^2 - m_{11} c_2 \tag{29}$$

spanwise momentum equation,

$$\frac{\partial}{\partial \eta}\left[b \frac{\partial G}{\partial \eta}\right] + \sigma_2 \frac{\partial G}{\partial \eta} + m_7 \left(\frac{\partial g}{\partial y_{le}} \frac{\partial G}{\partial \eta} - G \frac{\partial G}{\partial y_{le}}\right)$$

$$+ m_{10} \left(\frac{\partial f}{\partial s_r} \frac{\partial G}{\partial \eta} - F \frac{\partial G}{\partial s_r}\right) = m_9 F^2 + m_4 FG + m_3 G^2 - m_{12} c_2 \tag{30}$$

energy equation,

$$\frac{\partial}{\partial \eta}\left[\sigma_1 \frac{\partial E}{\partial \eta}\right] + \sigma_2 \frac{\partial E}{\partial \eta} + m_7 \left(\frac{\partial g}{\partial y_{le}} \frac{\partial E}{\partial \eta} - G \frac{\partial E}{\partial y_{le}}\right)$$

$$+ m_{10} \left(\frac{\partial f}{\partial s_r} \frac{\partial E}{\partial \eta} - F \frac{\partial E}{\partial s_r}\right) + \frac{\partial}{\partial \eta}\left[\sigma_4 \frac{\partial F}{\partial \eta}\right] + \frac{\partial}{\partial \eta}\left[\sigma_5 \frac{\partial G}{\partial \eta}\right] = 0 \tag{31}$$

where,

$$E = \frac{H}{H_e} \quad , \; c_1 = \frac{\rho\mu}{\rho_e \mu_e} \quad , \quad c_2 = \frac{\rho_e}{\rho}$$

$$b = c_1 \left(1 + \varepsilon_m^+\right) \quad , \; \varepsilon_m^+ = \varepsilon_m / \nu \tag{32}$$

The coefficients m_1-m_{12} are given by,

$$m_1 = \frac{1}{2h_1}\left(h_1 + \beta_3 + \beta_7\right) + \frac{s}{h_1}\left(\cot\Theta \frac{\partial \Theta}{\partial s_r} + \frac{1}{h_2}\frac{\partial h_2}{\partial s_r}\right)$$

$$m_2 = \frac{\beta_3}{h_1} - s\, K_1 \cot\Theta$$

$$m_3 = - s\, K_2 \cot\Theta\, \beta_2$$

$$m_4 = s\, K_{21}$$

$$m_5 = \frac{\beta_2 \beta_4}{h_2} + s\, K_{12}\, \beta_2$$

$$m_6 = \frac{\beta_2}{2h_2}\left(\frac{\partial s}{\partial y_{1e}} + \beta_8 - \beta_4\right) + \frac{s\,\beta_2}{h_2}\left(\cot\Theta \frac{\partial \Theta}{\partial y_{1e}} + \frac{1}{h_1}\frac{\partial h_1}{\partial y_{1e}}\right)$$

$$m_7 = \frac{s\,\beta_2}{h_2}$$

$$m_8 = s\, K_2 \csc\Theta\, \beta_2^{\,2}$$

$$m_9 = s\, K_1 \csc\Theta / \beta_2$$

$$m_{10} = \frac{s}{h_1}$$

$$m_{11} = \frac{\beta_3}{h_1} + \frac{\beta_1\beta_4}{h_2} + s\left(-K_1 \cot\Theta + K_2 \csc\Theta\, \beta_1^{\,2} + K_{12}\, \beta_1\right)$$

$$m_{12} = \frac{\beta_5}{h_1} + \frac{\beta_1\beta_6}{h_2} + \frac{s}{\beta_2}\left(-K_2 \cot\Theta\, \beta_1^{\,2} + K_1 \csc\Theta + K_{21}\, \beta_1\right) \tag{33}$$

and the coefficients σ_1-σ_5 are defined as,

$$\sigma_1 = \frac{c_1}{Pr}\left(1 + \varepsilon_m^+ \frac{Pr}{Pr_t}\right)$$

$$\sigma_2 = m_1\, f + m_6\, g$$

$$\sigma_3 = \frac{c_1\, u_e^{\,2}}{H_e}\left(1 - \frac{1}{Pr}\right)$$

$$\sigma_4 = \sigma_3\,(F + G\cos\Theta\, \beta_2)$$

$$\sigma_5 = \sigma_3\, \beta_2\,(G\, \beta_2 + F\cos\Theta) \tag{34}$$

where β_1-β_8 are the inviscid parameters,

$$\beta_1 = \frac{v_e}{u_e} \qquad \beta_2 = \frac{u_{ref}}{u_e}$$

$$\beta_3 = \frac{s}{u_e}\frac{\partial u_e}{\partial s_r} \qquad \beta_4 = \frac{s}{u_e}\frac{\partial u_e}{\partial y_{le}}$$

$$\beta_5 = \frac{s}{u_{ref}}\frac{\partial v_e}{\partial s_r} \qquad \beta_6 = \frac{s}{u_{ref}}\frac{\partial v_e}{\partial y_{le}}$$

$$\beta_7 = \frac{s}{\rho_e\mu_e}\frac{\partial}{\partial s_r}(\rho_e\mu_e) \qquad \beta_8 = \frac{s}{\rho_e\mu_e}\frac{\partial}{\partial y_{le}}(\rho_e\mu_e) \tag{35}$$

Next, define the vectors Z and ζ by,

$$Z = \begin{bmatrix} F \\ G \end{bmatrix}, \quad \zeta = \begin{bmatrix} f \\ g \end{bmatrix} \tag{36}$$

Then, using eq. (36), eqs. (27) and (28) may be combined and rewritten as the vector equation,

$$Z = \frac{\partial \zeta}{\partial \eta} \tag{37}$$

Also, eqs. (29) and (30) may be combined and written as,

$$\frac{\partial}{\partial \eta}\left[b \frac{\partial Z}{\partial \eta}\right] + \sigma_2 \frac{\partial Z}{\partial \eta} + m_7 \left(\frac{\partial g}{\partial y_{1e}} \frac{\partial Z}{\partial \eta} - G \frac{\partial Z}{\partial y_{1e}}\right)$$

$$+ m_{10} \left(\frac{\partial f}{\partial s_r} \frac{\partial Z}{\partial \eta} - F \frac{\partial Z}{\partial s_r}\right) = \Gamma_1 F^2 + \Gamma_2 FG + \Gamma_3 G^2 - \Gamma_4 c_2 \tag{38}$$

where,

$$\Gamma_1 = \begin{bmatrix} m_2 \\ m_9 \end{bmatrix} \quad , \Gamma_2 = \begin{bmatrix} m_5 \\ m_4 \end{bmatrix} \quad , \quad \Gamma_3 = \begin{bmatrix} m_8 \\ m_3 \end{bmatrix} \quad , \quad \Gamma_4 = \begin{bmatrix} m_{11} \\ m_{12} \end{bmatrix} \tag{39}$$

The boundary conditions for eqs. (37) and (38) are,

$$\eta = 0 \ : \ Z = \zeta = \begin{bmatrix} 0 \\ 0 \end{bmatrix} \quad , \quad \left(\frac{\partial E}{\partial \eta}\right)_w = 0$$

$$\eta = \eta_e \ : \ Z = \begin{bmatrix} 1 \\ v_e/u_{ref} \end{bmatrix} \quad , \quad E = 1 \tag{40}$$

Along the wing tip the spanwise derivatives of the flow variables are set equal to zero. Thus, the inviscid and geometric terms which are different from the general three-dimensional case are:

$$\beta_4 = \beta_6 = \beta_8 = 0$$

$$m_5 = s K_{12} \beta_2$$

$$m_6 = \frac{\beta_2}{h_2}\left[\frac{1}{2} \frac{\partial s}{\partial y_{1e}} + s \left(\cot\Theta \frac{\partial \Theta}{\partial y_{1e}} + \frac{1}{h_1} \frac{\partial h_1}{\partial y_{1e}}\right)\right]$$

$$m_{11} = \frac{\beta_3}{h_1} + s \left(- K_1 \cot\Theta + K_2 \csc\Theta \beta_1^2 + K_{12} \beta_1\right)$$

$$m_{12} = \frac{\beta_5}{h_1} + \frac{s}{\beta_2}\left(- K_2 \cot\Theta \beta_1^2 + K_1 \csc\Theta + K_{21} \beta_1\right) \tag{41}$$

and the governing equations reduce to,

$$\frac{\partial}{\partial\eta}\left[b\,\frac{\partial Z}{\partial\eta}\right] + \sigma_2\,\frac{\partial Z}{\partial\eta} + m_{10}\left(\frac{\partial f}{\partial s_r}\,\frac{\partial Z}{\partial\eta} - F\,\frac{\partial Z}{\partial s_r}\right)$$

$$= \Gamma_1 F^2 + \Gamma_2 FG + \Gamma_3 G^2 - \Gamma_4 c_2 \tag{42}$$

$$\frac{\partial}{\partial\eta}\left[\sigma_1\,\frac{\partial E}{\partial\eta}\right] + \sigma_2\,\frac{\partial E}{\partial\eta} + m_{10}\left(\frac{\partial f}{\partial s_r}\,\frac{\partial E}{\partial\eta} - F\,\frac{\partial E}{\partial s_r}\right)$$

$$+ \frac{\partial}{\partial\eta}\left[\sigma_4\,\frac{\partial F}{\partial\eta}\right] + \frac{\partial}{\partial\eta}\left[\sigma_5\,\frac{\partial G}{\partial\eta}\right] = 0 \tag{43}$$

The boundary conditions for the above are the same as those given by eq. (40).

For the flow along the root-chord line, the same transformation as that used for the general case will be employed. However, the stream functions are defined in a slightly different manner,

$$\rho u h_2 \sin\Theta = \frac{\partial\psi}{\partial n}\,,\quad \rho h_1 \sin\Theta\, v_y = \frac{\partial\phi}{\partial n}\,,\quad \overline{\rho w}\, h_1 h_2 \sin\Theta = -\left(\frac{\partial\psi}{\partial s_r} + \phi\right) \tag{44}$$

so that eq. (13) is satisfied identically. Using eqs. (23), (25) and (26) in the above yields the velocity profiles for the flow along the root-chord line,

$$\frac{u}{u_e} = \frac{\partial f}{\partial\eta} = F \tag{45}$$

$$\frac{v_y}{u_{ref}} = \frac{\partial g}{\partial\eta} = G \tag{46}$$

The governing equations along the root-chord line may be written as eqs. (42) and (43) provided that,

$$m_3 = s\,\beta_2/h_2$$

$$m_5 = m_8 = 0$$

$$m_6 = m_3$$

$$m_9 = \frac{s}{\beta_2}\,\frac{\partial}{\partial y_{le}}\,(K_1 \csc\Theta)$$

$$m_{11} = m_2$$

$$m_{12} = \frac{s}{u_{ref}} \left[\frac{1}{h_1} \frac{\partial v_{ye}}{\partial s_r} + \frac{1}{h_2} \frac{v_{ye}^2}{u_e} + K_{21}\, v_{ye} + u_e \frac{\partial}{\partial y_{le}} (K_1 \csc\Theta)\right]$$

$$\sigma_4 = \sigma_3\, F$$

$$\sigma_5 = 0 \tag{47}$$

where the boundary conditions are now given by,

$$\eta = 0 \quad : \quad Z = \zeta = \begin{bmatrix} 0 \\ 0 \end{bmatrix} \quad , \quad \left(\frac{\partial E}{\partial \eta}\right)_w = 0$$

$$\eta = \eta_e \quad : \quad Z = \begin{bmatrix} 1 \\ v_{ye}/u_{ref} \end{bmatrix} \quad , \quad E = 1 \tag{48}$$

Along the attachment line of the wing both s and u_e are zero. Therefore, the governing attachment-line equations are transformed by defining η as,

$$\eta = \left(\frac{u_{se}}{\nu_e h_1}\right)^{1/2} \int_0^n \frac{\rho}{\rho_e}\, dn \tag{49}$$

and ψ and ϕ are now given by,

$$\psi = (\rho_e \mu_e u_{se} h_1)^{1/2} h_2 \sin\Theta\, f \tag{50}$$

$$\phi = \left(\frac{\rho_e \mu_e h_1}{u_{se}}\right)^{1/2} u_{ref} h_1 \sin\Theta\, g \tag{51}$$

For the flow along the attachment line the stream functions must satisfy the relations,

$$\rho h_2 \sin\Theta\, u_s = \frac{\partial \psi}{\partial n} \, , \quad \rho v h_1 \sin\Theta = \frac{\partial \phi}{\partial n} \, ,$$

$$\overline{\rho w}\, h_1 h_2 \sin\Theta = -\left(\psi + \frac{\partial \phi}{\partial y_{le}}\right) \tag{52}$$

Using eqs. (49)-(51) in eq. (52) yields the velocity profiles for the flow along the attachment line as,

$$\frac{u_s}{u_{se}} = \frac{\partial f}{\partial \eta} = F \tag{53}$$

$$\frac{v_e}{u_{ref}} = \frac{\partial g}{\partial \eta} = G \tag{54}$$

With the above, the governing (laminar) attachment-line equations become,

$$\frac{\partial}{\partial \eta}\left[c_1 \frac{\partial Z}{\partial \eta}\right] + \sigma_2 \frac{\partial Z}{\partial \eta} + m_7 \left(\frac{\partial g}{\partial y_{le}} \frac{\partial Z}{\partial \eta} - G \frac{\partial Z}{\partial y_{le}}\right)$$

$$= \Gamma_1 F^2 + \Gamma_2 FG + \Gamma_3 G^2 - \Gamma_4 c_2 \tag{55}$$

$$\frac{\partial}{\partial \eta}\left[\sigma_1 \frac{\partial E}{\partial \eta}\right] + \sigma_2 \frac{\partial E}{\partial \eta} + m_7 \left(\frac{\partial g}{\partial y_{le}} \frac{\partial E}{\partial \eta} - G \frac{\partial E}{\partial y_{le}}\right) + \frac{\partial}{\partial \eta}\left[\sigma_5 \frac{\partial G}{\partial \eta}\right] = 0 \tag{56}$$

The boundary conditions for the attachment-line equations are the same as those for the general case. The inviscid and geometry coefficients are now given by,

$$m_1 = m_2 = 1$$

$$m_3 = - h_1 K_2 \gamma_2 \cot\Theta$$

$$m_4 = m_9 = 0$$

$$m_5 = \frac{\gamma_2 \gamma_3}{h_2} + h_1 K_{12} \gamma_2$$

$$m_6 = \gamma_2 \left[\frac{h_1}{h_2} \cot\Theta \frac{\partial \Theta}{\partial y_{le}} + \frac{3}{2h_2} \frac{\partial h_1}{\partial y_{le}} + \frac{1}{2h_2} (\gamma_5 - \gamma_3)\right]$$

$$m_7 = \frac{h_1 \gamma_2}{h_2}$$

$$m_8 = h_1 \gamma_2^2 \frac{\partial}{\partial s_r} (K_2 \csc\Theta)$$

$$m_{11} = 1 + \frac{\gamma_1\gamma_3}{h_2} + h_1 K_{12}\gamma_1 + h_1\gamma_1^2 \frac{\partial}{\partial s_r}(K_2 \csc\Theta)$$

$$m_{12} = \frac{\gamma_1\gamma_4}{h_2} - h_1 K_2 \cot\Theta\ \gamma_1^2/\gamma_2 \qquad (57)$$

$$\sigma_1 = \frac{c_1}{Pr}$$

$$\sigma_3 = \frac{c_1\ u_{ref}^2}{H_e}\left(1 - \frac{1}{Pr}\right) \qquad (58)$$

$$\sigma_5 = \sigma_3\ G$$

where the terms $\gamma_1 - \gamma_5$ are,

$$\gamma_1 = \frac{v_e}{u_{se}} \quad , \quad \gamma_2 = \frac{u_{ref}}{u_{se}}$$

$$\gamma_3 = \frac{h_1}{u_{se}} \frac{\partial u_{se}}{\partial y_{le}} \quad , \quad \gamma_4 = \frac{h_1}{u_{ref}} \frac{\partial v_e}{\partial y_{le}}$$

$$\gamma_5 = \frac{h_1}{\rho_e u_e} \frac{\partial}{\partial y_{le}}(\rho_e \mu_e) \qquad (59)$$

Applying the transformation given by eqs. (23)-(28) to the eddy-viscosity formulas given by eq. (7) yields,

$$(\varepsilon_m^+)_i = \left(\frac{\nu_e}{\nu}\right)\sqrt{Re}\ \frac{1}{c_2}\left[0.4\int_o^\eta c_2\, d\eta\right]^2 \left[1 - \exp\left(-\frac{\eta}{A}\right)\right]^2$$

$$*\left[\left(\frac{\partial F}{\partial \eta}\right)^2 + \beta_2^2\left(\frac{\partial G}{\partial \eta}\right)^2 + 2\beta_2 \cos\Theta \frac{\partial F}{\partial \eta}\frac{\partial G}{\partial \eta}\right]^{1/2} \qquad (60a)$$

$$(\varepsilon_m^+)_o = \left(\frac{\nu_e}{\nu}\right)\sqrt{Re}\ (0.0168)\left|\int_o^{\eta_e} c_2\left[\sqrt{1 + \beta_1^2 + 2\beta_1 \cos\Theta}\right.\right.$$

$$- \sqrt{F^2 + (\beta_2 G)^2 + 2\,\beta_2 \cos\Theta\, FG}\ ]\, d\eta \Big| \qquad (60b)$$

where Re is a local Reynolds number and,

$$\frac{\eta}{A} = \left(\frac{\nu_e}{\nu}\right) \sqrt{c_{1w}\, c_2}\, \left(\frac{1}{2\delta}\right) Re^{1/4} \int_0^{\eta} c_2\, d\eta \left[\left(\frac{\partial F}{\partial \eta}\right)_w^2 + \beta_2{}^2 \left(\frac{\partial G}{\partial \eta}\right)_w^2 + 2\,\beta_2 \cos\Theta \left(\frac{\partial F}{\partial \eta}\right)_w \left(\frac{\partial G}{\partial \eta}\right)_w\right]^{1/4} \qquad (61)$$

FINITE-DIFFERENCE TECHNIQUE

The transformed governing equations are differenced using a second-order accurate predictor-corrector scheme originally developed by Matsuno [6]. The scheme is implicit in the normal direction and explicit in the spanwise direction. It was demonstrated by Woodson and DeJarnette [11] to yield accurate numerical results when compared to the exact solution of the three-dimensional boundary-layer equations for parabolic flow over a moving flat plate. An advantage of this method over other methods used to solve the three-dimensional boundary-layer equations [2,5] is that the crossflow derivatives are formed independent of the sign of the crossflow velocity component. The finite-difference cell is illustrated in figure 3.

The notation $Z_{i,j,k} = Z\,(s_{r_i}, y_{le_j}, \eta_k)$ is employed, where,

$$s_{r_{i+1}} = s_{r_i} + \Delta s_{r_i} \quad , \quad i = 1,2,\ldots IMAX$$

$$y_{le_{j+1}} = y_{le_j} + \Delta y_{le} \quad , \quad j = 1,2,\ldots JMAX$$

$$\eta_{k+1} = \eta_k + \Delta\eta_k \quad , \quad k = 1,2,\ldots KMAX \qquad (62)$$

A coordinate stretching procedure developed by Blottner [12] is used in the normal direction so that the mesh is clustered near the surface of the wing. Central difference operators are defined by the relations,

$$\delta_\eta Z_{i,j,k} = (Z_{i,j,k+1} - Z_{i,j,k-1})/(\Delta\eta_k + \Delta\eta_{k-1}) \qquad (63)$$

$$\delta_y Z_{i,j,k} = (Z_{i,j+1,k} - Z_{i,j-1,k})/2\Delta y_{le} \qquad (64)$$

$$\Delta_\eta Z_{i,j,k-1/2} = (Z_{i,j,k} - Z_{i,j,k-1})/\Delta\eta_{k-1} \tag{65}$$

$$\Delta_s Z_{i+1/2,j,k} = (Z_{i+1,j,k} - Z_{i,j,k})/\Delta s r_i \tag{66}$$

$$\Delta_\eta [b_{i,j,k} \Delta_\eta Z_{i,j,k}] = 2 [b_{i,j,k+1/2} (Z_{i,j,k+1} - Z_{i,j,k})/\Delta\eta_k$$

$$- b_{i,j,k-1/2} (Z_{i,j,k} - Z_{i,j,k-1})/\Delta\eta_{k-1}]/(\Delta\eta_k + \Delta\eta_{k-1}) \tag{67}$$

and a backward difference operator for the predictor step by,

$$\nabla_s Z_{i+1/2,j,k} = 2 (Z_{i+1/2,j,k} - Z_{i,j,k})/\Delta s r_i \tag{68}$$

where,

$$b_{i,j,k\pm1/2} = (b_{i,j,k} + b_{i,j,k\pm1})/2 \tag{69}$$

Applying the above operations at the predictor step to eqs. (37), (38), and (31) they become, respectively:

$$\Delta_\eta \zeta_{i+1/2,j,k-1/2} = Z_{i+1/2,j,k-1/2} \tag{70}$$

$$\Delta_\eta [b_{i,j,k} \Delta_\eta Z_{i+1/2,j,k}] + \sigma_{2_{i,j,k}} \delta_\eta Z_{i,j,k}$$

$$+ m_7 (\delta_y g_{i,j,k} \delta_\eta Z_{i,j,k} - G_{i,j,k} \delta_y Z_{i,j,k})$$

$$+ m_{10} (\nabla_s f_{i+1/2,j,k} \delta_\eta Z_{i,j,k} - F_{i,j,k} \nabla_s Z_{i+1/2,j,k})$$

$$= [\Gamma_1 F^2 + \Gamma_2 FG + \Gamma_3 G^2 - \Gamma_4 c_2]_{i,j,k} \tag{71}$$

$$\Delta_\eta \left[\sigma_{1_{i,j,k}} \Delta_\eta E_{i+1/2,j,k}\right] + \sigma_{2_{i,j,k}} \delta_\eta E_{i,j,k}$$

$$m_7 \left(\delta_y g_{i,j,k} \delta_\eta E_{i,j,k} - G_{i,j,k} \delta_y E_{i,j,k}\right)$$

$$+ m_{10} \left(\nabla_s f_{i+1/2,j,k} \delta_\eta E_{i,j,k} - F_{i,j,k} \nabla_s E_{i+1/2,j,k}\right)$$

$$+ \Delta_\eta \left[\sigma_{4_{i,j,k}} \Delta_\eta F_{i,j,k}\right] + \Delta_\eta \left[\sigma_{5_{i,j,k}} \Delta_\eta G_{i,j,k}\right] = 0 \qquad (72)$$

and at the corrector step they are given by:

$$\Delta_\eta \zeta_{i+1,j,k-1/2} = Z_{i+1,j,k-1/2} \qquad (73)$$

$$\Delta_\eta \left[b_{i+1/2,j,k} \Delta_\eta \left(Z_{i+1,j,k} + Z_{i,j,k}\right)/2\right] + \sigma_{2_{i+1/2,j,k}} \delta_\eta Z_{i+1/2,j,k}$$

$$+ m_7 \left(\delta_y g_{i+1/2,j,k} \delta_\eta Z_{i+1/2,j,k} - G_{i+1/2,j,k} \delta_y Z_{i+1/2,j,k}\right)$$

$$+ m_{10} \left(\Delta_s f_{i+1/2,j,k} \delta_\eta Z_{i+1/2,j,k} - F_{i+1/2,j,k} \Delta_s Z_{i+1/2,j,k}\right)$$

$$= \left[\Gamma_1 F^2 + \Gamma_2 FG + \Gamma_3 G^2 - \Gamma_4 c_2\right]_{i+1/2,j,k} \qquad (74)$$

$$\Delta_\eta \left[\sigma_{1_{i+1/2,j,k}} \Delta_\eta \left(E_{i+1,j,k} + E_{i,j,k}\right)/2\right] + \sigma_{2_{i+1/2\,j,k}} \delta_\eta E_{i+1/2,j,k}$$

$$+ m_7 \left(\delta_y g_{i+1/2,j,k} \delta_\eta E_{i+1/2,j,k} - G_{i+1/2,j,k} \delta_y E_{i+1/2,j,k}\right)$$

$$+ m_{10} \left(\Delta_s f_{i+1/2,j,k} \delta_\eta E_{i+1/2,j,k} - F_{i+1/2,j,k} \Delta_s E_{i+1/2,j,k}\right)$$

$$+ \Delta_\eta \left[\sigma_{4_{i+1/2,j,k}} \Delta_\eta F_{i+1/2,j,k}\right]$$

$$+ \Delta_\eta \left[\sigma_{5_{i+1/2,j,k}} \Delta_\eta G_{i+1/2,j,k} \right] = 0 \tag{75}$$

The inviscid and geometry parameters are evaluated at the $(i+1/2, j)$ station for both the predictor and corrector steps. After performing the indicated operations, eqs. (70)-(75) may be written as a set of linear algebraic equations,

$$\zeta_{j,k} = \zeta_{j,k-1} + \frac{\Delta\eta_{k-1}}{2} \left(Z_{j,k} + Z_{j,k-1} \right) \tag{76}$$

$$- a_m Z_{j,k-1} + b_m Z_{j,k} - c_m Z_{j,k+1} + d_m \zeta_{j,k} = e_m \tag{77}$$

$$- a_e E_{j,k-1} + b_e E_{j,k} - c_e E_{j,k+1} = d_e \tag{78}$$

where a_m, c_m, a_e, b_e, c_e, and d_e are scalars, b_m and d_m are 2 by 2 coefficient matricies and e_m is a vector. Their values are provided in Appendix C. Equations (76) and (77) are block tridiagonal equations and can be solved using a block form of the Davis modified tridiagonal algorthim [13]. Equation (78) is a linear tridiagonal equation and may be solved by the Thomas algorithm [14].

The infinite-swept-wing equations, root-chord line equations and attachment-line equations may each be written in the form of eqs. (76)-(78). They produce a set of coefficients which are subsets of the ones given in Appendix C so their values are not listed here.

The character of the three-dimensional boundary-layer equations was shown by Raetz [15] to be of a parabolic nature with secondary hyperbolic-like properties. This led Raetz to formulate the well-known zones of influence and dependence concept. The concept simply stated is that a disturbance at a point p is instantly felt by all points on a vertical line passing through p and then convected downstream along all streamlines passing through that point. Since the direction of the streamlines varies across the boundary layer, it is possible to identify the regions of influence and dependence of a particular point. The effect of the zone of dependence on the numerical calculations is to limit the allowable marching step size. Before the solution can be advanced from one streamwise plane to the next, the maximum step size must be determined from the relation [16],

$$\Delta s_r < \underset{\text{all } j,k}{\text{Minimum}} \left\{ \Delta y_{le} \frac{u}{|v|} \frac{h_2}{h_1} \right\} \tag{79}$$

For the present method, the spanwise step size is chosen to be a constant and the marching step size is calculated along with the viscous solution. The solution begins at the root-chord of the wing and proceeds spanwise, along the attachment line, from the root to the tip using the attachment-line equations.

With an initial solution thus provided, the fully three-dimensional equations are marched streamwise from the attachment line, around the leading edge, to the upper surface trailing edge, and then from the attachment line to the lower surface trailing edge. The solution along the root- and tip-chord lines is obtained in the same manner by solving the root-chord line equations and infinite-swept-wing equations, respectively, and provides the side boundary conditions for the three-dimensional equations.

BOUNDARY-LAYER PARAMETERS

When the viscous solution has been determined, skin-friction coefficients, inviscid and viscous streamlines, and the three-dimensional displacement surface are calculated. A streamwise skin-friction coefficient is defined by,

$$C_{f_s} = \frac{2\,\tau_s}{\rho_\infty\, u_\infty^2} \tag{80a}$$

and a spanwise skin-friction coefficient by,

$$C_{f_y} = \frac{2\,\tau_y}{\rho_\infty\, u_\infty^2} \tag{80b}$$

Using the transformation given by eqs. (23)-(28) the skin-friction coefficients become,

$$C_{f_s} = \frac{2c_{1w}}{\sqrt{Re}} \left(\frac{\rho_e}{\rho_\infty}\right) \left(\frac{u_e}{u_\infty}\right)^2 \left(\frac{\partial F}{\partial \eta}\right)_w \tag{81a}$$

$$C_{f_y} = \frac{2c_{1w}}{\sqrt{Re}} \left(\frac{\rho_e}{\rho_\infty}\right)\left(\frac{u_e\, u_{ref}}{u_\infty^2}\right) \left(\frac{\partial G}{\partial \eta}\right)_w \tag{81b}$$

The limiting streamline angle, β_w, is defined as

$$\beta_w = \tan^{-1}\left(C_{f_y}/C_{f_s}\right) \tag{82}$$

Therefore, the equation for the surface streamlines in the (s,y)-plane is given by

$$\left(\frac{dy}{ds}\right)_w = \tan \beta_w \tag{83a}$$

so that in the $(\bar{x},\bar{y})$-plane the above becomes

$$\left(\frac{d\bar{y}}{d\bar{x}}\right)_w = \left[\frac{\cos\Omega\ \cos\Lambda}{\cos\kappa}\right] \tan\beta_w \tag{83b}$$

A streamwise and a spanwise velocity integral thickness are defined as,

$$\delta_s^* = \int_0^\infty \left(1 - \frac{\rho u}{\rho_e u_e}\right) dn \tag{84a}$$

$$\delta_y^* = \int_0^\infty \left(1 - \frac{\rho v}{\rho_e v_e}\right) dn \tag{84b}$$

In transformed coordinates the velocity integral thicknesses become,

$$\delta_s^* = \frac{s}{\sqrt{Re}} \left[\int_0^{\eta_e} c_2 d\eta - f(\eta_e)\right] \tag{85a}$$

$$\delta_y^* = \frac{s}{\sqrt{Re}} \left[\int_0^{\eta_e} c_2\ d\eta - \frac{u_{ref}}{v_e}\ g\ (\eta_e)\right] \tag{85b}$$

The three-dimensional displacement surface, Δ^*, was defined by Moore [17] to be the solution of the equation,

$$\nabla \cdot \left[\rho_e \vec{V}_e\ \Delta^* - \int_0^\infty (\rho_e \vec{V}_e - \rho\vec{V})\ dn\right] = 0$$

$$\frac{\partial}{\partial s_r} \left[\rho_e\ u_e\ h_2\ \sin\Theta\ (\Delta^* - \delta_s^*)\right]$$

$$+ \frac{\partial}{\partial y_{le}} \left[\rho_e\ v_e\ h_1\ \sin\Theta\ (\Delta^* - \delta_y^*)\right] = 0 \tag{86}$$

When the displacement surface has been calculated for both the upper and lower surfaces of the wing, a new wing surface is defined by adding the displacement surface to the original wing coordinates, and the inviscid solution is then determined for the new wing surface. The displacement surface is not smoothed, but is slightly under-relaxed during the first few viscous updates. This procedure (global iteration) is repeated until the viscous updates are less than some user-specified tolerance. On the plane of symmetry the boundary-layer parameters are given by,

$$C_{f_s} = \frac{2c_{1w}}{\sqrt{Re}} \left(\frac{\rho_e}{\rho_\infty}\right) \left(\frac{u_e}{u_\infty}\right)^2 \left(\frac{\partial F}{\partial \eta}\right)_w \tag{87a}$$

$$C_{f_y} = 0 \tag{87b}$$

$$\delta_s^* = \frac{s}{\sqrt{Re}} \left[\int_0^{\eta_e} c_2 \, d\eta - f(\eta_e) \right] \tag{88a}$$

$$\delta_y^* = \frac{s}{\sqrt{Re}} \left[\int_0^{\eta_e} c_2 \, d\eta - \frac{u_{ref}}{v_{ye}} g(\eta_e) \right] \tag{88b}$$

and along the attachment line they are given by,

$$C_{f_s} = 0 \tag{89a}$$

$$C_{f_y} = 2 \, c_{1w} \left(\frac{\nu_e}{u_{se} \, h_1} \right)^{1/2} \left(\frac{\rho_e}{\rho_\infty} \right) \left(\frac{u_{ref} \, u_{se}}{u_\infty^2} \right) \left(\frac{\partial G}{\partial \eta} \right)_w \tag{89b}$$

$$\delta_s^* = \left(\frac{\nu_e \, h_1}{u_{se}} \right)^{1/2} \left[\int_0^{\eta_e} c_2 \, d\eta - f(\eta_e) \right] \tag{90a}$$

$$\delta_y^* = \left(\frac{\nu_e \, h_1}{u_{se}} \right)^{1/2} \left[\int_0^{\eta_e} c_2 \, d\eta - \frac{u_{ref}}{v_e} g(\eta_e) \right] \tag{90b}$$

DISCUSSION OF RESULTS

The inviscid solution is determined on a grid which consists of 160 grid points in the streamwise direction, 32 points spanwise and 24 points normal to the wing-fuselage surface. For the viscous solution a total of 110 streamwise and 31 spanwise grid points are used for both the upper and lower surfaces of the wing. The number of grid points across the boundary layer varies from 26 at the attachment line to about 75 at the trailing edge. Each of the calculations presented here was performed on a Gould PN 9005 computer which has an operating speed of 0.8 MFLOPS.

As a test case for the present method, a solution was calculated for flow over a swept and tapered wing attached to a cylindrical fuselage. The wing has a aspect ratio of eight and a NACA 0012 cross-section, without twist. The planform is given in figure 4 and has a taper ratio of 0.5 and a leading-edge sweep angle of 20 degrees. The solution was determined for a Mach number of $M_\infty = 0.85$ with the wing at an angle of attack of two degrees and a Reynolds number based on the mean aerodynamic chord of nine million. The results of

the present method are compared to those obtained using the TAWFIVE computer code developed by Streett and Melson [9], and to the inviscid results from FLO-30. For simplicity, the present method will henceforth be referred to by the acronym TIBLT (for Transonic Interactive Boundary-Layer Theory).

In order to directly compare the two inviscid-viscous interaction methods, the boundary layer was assumed to transition from laminar to turbulent flow at the first marching step beyond the attachment line. Both methods employ
FLO-30 as the inviscid solver, but the viscous routine in TAWFIVE is an integral method while TIBLT solves the boundary-layer equations in the differential form. Twelve viscous updates were performed by both interaction methods and the number of inviscid iterations was the same for all three calculations.

Figure 5 compares the streamwise distribution of the pressure coefficient determined by the three calculation methods. The effect of the boundary layer moves the location of the upper surface shock wave towards the leading edge, reduces the strength of the shock, and decreases the static pressures in the trailing-edge region. The location of the shock wave moves forward as the wing tip is approached and near the tip the shock location is nearly identical for both of the interaction methods. This may be due to the fact that both methods make an infinite-swept-wing assumption at the wing tip. Due to the location of the shock wave, upper surface boundary layer separation was predicted at $\xi = 0.505$ for the TAWFIVE calculation and at $\xi = 0.510$ for TIBLT.

The determination of boundary layer separation is different for the two interaction methods. Since TAWFIVE is an integral boundary-layer method, the criterion for separation is when the compressible shape factor reaches a critical value of 2.8 [9]. On the other hand, in TIBLT separation is indicated when the streamwise skin-friction coefficient goes through zero. Neither criteria can be said to be the absolute definition of three-dimensional boundary-layer separation, however, they may be thought of as indicators that separation is imminent [18-21]. When separation is encountered in the TIBLT calculation the displacement surface is calculated from the separation line to the trailing edge by assuming the terms in the brackets in eq. (85) to be constant and equal to their values at separation. The lift and drag coefficients computed by each of the calculation methods is presented in table 1. Both the lift and drag were slightly larger for the TIBLT calculation than for the TAWFIVE calculation.

Table 1- Lift and Drag Coefficients for NACA 0012 Wing

	FLO-30	TAWFIVE	TIBLT
C_L	0.302	0.248	0.275
C_D	0.0172	0.0175	0.0181

As a further test for TIBLT, a subcritical and a supercritical Mach number solution were calculated for the ONERA M6 wing for which experimental results are available [22]. In both cases the angle of attack was 3.06 degrees and the freestream Reynolds number was 11.7 million, based on the mean aerodynamic chord. The M6 wing has an aspect ratio of 3.8, a taper ratio of 0.56, and a leading edge sweep angle of 30 degrees. The planform is shown in figure 6. The subcritical Mach number was $M_\infty = 0.699$ and a comparison of the streamwise distribution of the pressure coefficient determined by TIBLT and TAWFIVE with the experiment of reference 22 is given in figure 7. Viscous effects are moderate for this case and both interaction methods compare favorably with the measured values.

Five viscous updates were performed by both interaction methods. The computer run time for the TAWFIVE calculation was 5.64 CPU-hours while the run time for the TIBLT calculation was 21.87 CPU-hours, approximately 3.9 times that of TAWFIVE. This difference may be accounted for by noting that in the integral method the shape of the velocity profiles is assumed a priori, while in the differential method they are determined as part of the solution. The additional calculations performed across the boundary layer at each marching step for the differential method results in the longer run times.

Typical velocity and total enthalpy profiles from the TIBLT calculation are provided in figure 8. The spanwise velocity profile exhibits velocity crossover; the velocity component is positive near the wing surface and negative at the edge of the boundary layer. This type of velocity profile can not be modeled by the TAWFIVE code, nor by most integral methods and illustrates an advantage of differential methods over integral methods. The locations where this type of spanwise profile occurs on the upper surface of the wing is shown in figure 9. The dark triangles in the figure are the places where the spanwise profile exhibits velocity crossover. The majority of the spanwise profiles along the root chord line have velocity crossover. The chordwise extent of this type of profile diminishes as the wing tip is approached, and the locations are concentrated near the trailing edge.

The supercritical solution was for a freestream Mach number of $M_\infty = 0.84$ and a comparison of the streamwise distribution of the pressure coefficient is presented in figure 10. Both interaction methods predict a weaker shock wave than the experiment and the computed locations of the shock are slightly forward of the experimentally observed location. The TIBLT code predicted a shock location somewhat closer to the experiment than the TAWFIVE code, except near the wing tip where, as in the NACA 0012 solution, the shock location is nearly identical for both interaction methods. Surprisingly, the TAWFIVE code predicted upper surface boundary-layer separation at $\xi = 0.209$, while no separation was predicted by the TIBLT code nor was there any indication of separation in the experiment.

Ten viscous updates were performed by both interaction methods and the computer run times were 7.82 and 44.53 CPU-hours for the TAWFIVE and TIBLT codes, respectively. Figure 11 shows the locations where the spanwise velocity profile has velocity crossover for the upper surface of the wing. Figure 11 is very similar to figure 9 except that the chordwise extent of the crossover profiles is smaller for the higher Mach number case. The angle of

attack and the Reynolds number were the same for both cases, thus the effect of increasing the Mach number does not change the distribution of the crossover profiles but does reduce the number of such profiles.

The present method was also applied to a Douglas Aircraft Company (DAC) wing-fuselage semispan model which was tested by Spaid and Roos [23,24] at the NASA-Ames Research Center 14-Foot Transonic Wind Tunnel. The wing has an aspect ratio of 6.8, a taper ratio of 0.3 and a quarter-chord sweep angle of 35 degrees. It employs 11.71 degrees of twist and the planform is shown in figure 12. Two experiments were conducted. The first was for a subcritical Mach number of $M_\infty = 0.5$, an angle of attack of six degrees, and a Reynolds number based on the mean aerodynamic chord of 3.4 million. The second test was for a Mach number of $M_\infty = 0.825$, an angle of attack of four degrees, and a Reynolds number of 4.5 million. A total of 378 static pressure orifices were located at nine spanwise stations on the primary wing. An auxiliary wing with a two-degree-of-freedom probe traversing unit was attached to the fuselage downstream of the primary wing. The probe traversing unit could be installed at any one of the nine spanwise locations on the auxiliary wing, thus allowing boundary-layer profiles to be obtained along each row of static pressure orifices. Spaid defined a local skin-friction coefficient and an inviscid yaw-plane flow-direction angle as,

$$C_f = \frac{2\,\tau_s}{\rho_e u_{Te}^2} \tag{91}$$

$$\beta_e = \tan^{-1}\left[\bar{v}_e/\bar{u}_e\right] \tag{92}$$

Thus, if β_e is positive, the inviscid flow is moving outboard towards the wing tip. It was intended to compare the results of both TAWFIVE and TIBLT with the experiment, however, the TAWFIVE code computed the displacement thickness on the lower surface of the wing to be unrealistically high and the solution became unstable. The TIBLT code had no difficulty in computing a solution for either Mach number and the results are presented below.

A comparison of the calculated and experimental upper surface pressure coefficient for the subcritical Mach number is given in figure 13. There is a very sharp pressure peak near the leading edge at the inner span stations. These large inviscid gradients had to be smoothed out slightly during the first few boundary-layer calculations to keep the surface flow attached. A total of five viscous updates were performed for this case and required 24.42 CPU-hours to run. The inviscid flow-direction angle is compared in figure 14 which shows the inviscid flow is moving inboard towards the wing root over 98% of the chord due to the wing twist. Figure 15 is a comparison of the local skin-friction coefficient and figure 16 compares the streamwise velocity integral-thickness distributions. The experimental skin-friction coefficient was determined by the Clauser chart technique [25] and the integral thickness

from the measured streamwise velocity profiles. The agreement between the calculated and experimental skin-friction coefficients is excellent at each of the span stations. The calculated streamwise velocity integral thickness agrees very well with the experiment near the wing tip, however, at the more highly loaded mid-semispan stations it is significantly under-predicted. This trend was also observed by Spaid [26] when he compared his experimental results to various two- and three-dimensional boundary-layer calculations. Figure 17 is a reproduction of figure 7 from reference 26 which shows the comparison of the experimental streamwise velocity integral thickness with the three-dimensional boundary-layer method of Cebeci, et al. [5]. The solid line in figure 17 is Cebeci's three-dimensional calculation and η is the percentage of the semispan. Cebeci used the experimental pressure distribution to drive his boundary-layer code but still under-predicted the experimental integral thickness at the mid-semispan station. The difference between the experiment and the boundary-layer methods is probably due to the transition location along the span and flow unsteadiness in the experiment.

In a recent paper, Cebeci and his co-workers [27] showed that moving the transition location has a significant effect on the displacement thickness distribution near the trailing edge. For the present method, the flow was assumed to be fully turbulent just prior to the location of the upper surface pressure peak, which occurs at about $\xi = 0.015$. Cebeci's calculation determined the transition location to be at $\xi = 0.025$. A challenge for three-dimensional boundary-layer methods is to properly account for the spanwise variation of the attachment line and transition location. At present, TIBLT determines an average constant-chord attachment line and assumes transition location. In the experiment, a boundary-layer trip was located on the upper surface at $\xi = 0.06$, which is aft of the sharp pressure peak so that they may have been trying to trip an already turbulent boundary layer. The precise location of the experimental transition line and its spanwise variation is not known, and may account for some of the observed difference between the boundary-layer methods and the experiment. Also, there was some flow unsteadiness in the experiment due to the mixing of the tunnel flow with the outside air which produced some probe vibrations on the auxiliary wing [23,28].

The locations where the spanwise velocity profile has velocity crossover on the upper surface of the wing is illustrated in figure 18. Once again the majority of the spanwise profiles near the root chord are of this type and as the wing tip is approached their chordwise extent diminishes and is concentrated near the trailing edge. The calculated inviscid and surface streamlines for the upper surface of the wing are presented in figure 19. The inviscid flow moves inboard as it goes over the wing due to the wing twist. The surface flow also moves inboard until just aft of the mid-chord line where it then begins to move slightly outboard, except near the root and tip where it continues inboard.

A comparison of the upper surface pressure coefficient for the super-critical Mach number is provided in figure 20. The shock location calculated by TIBLT is slightly forward of the experimental location at the inner span stations. At the outer span station no shock wave is present, probably due to the wing twist and to tip effects. A total of ten viscous updates were

performed and the calculation took 43.43 CPU-hours. The inviscid flow-inclination angle, skin-friction coefficient, and streamwise velocity integral thickness distributions are compared in figures 21, 22, and 23, respectively. The results for this supercritical case are very similar to those from the subcritical case. The locations where the spanwise velocity profile has velocity crossover on the upper surface of the wing is presented in figure 24. The number of these profiles is less than those for the subcritical case, but their distribution is similar. The calculated inviscid and surface streamlines for the upper surface are given in figure 25. The streamline patterns look the same as those from the subcritical case except for the surface flow near the wing root, which is moving farther inboard.

CONCLUSIONS

A method for determining the three-dimensional, laminar and turbulent boundary-layer flow over arbitrary swept wings was developed. The effect of the boundary layer on the inviscid solution is accounted for through a displacement surface interaction. The number of inviscid-viscous interactions required to obtain a converged solution varies depending on the flow conditions. Based on the results of the present study the following conclusions are drawn:

(1) The method is very general and may be applied to a wide variety of wing planforms provided the leading-edge sweep angle and taper ratio are not too severe, due to limitations of the inviscid grid.

(2) The finite-difference technique used to solve the three-dimensional boundary-layer equations has the advantage over other finite-difference schemes in that the crossflow difference formulas are formed independent of the sign of the crossflow velocity component.

(3) The method compared favorably with another inviscid-viscous interaction method and with experimental results for both subcritical and supercritical Mach numbers.

(4) In each of the cases considered, the spanwise velocity profile exhibited velocity crossover somewhere in the solution. The locations where this type of velocity profile occurs for a given wing planform are dependent on Mach number, Reynolds number, and angle of attack. An advantage of the present method over integral methods is that this type of spanwise velocity profile may be obtained as part of the solution without any special accommodation.

REFERENCES

1. Streett, C. L.: Viscous-Inviscid Interaction Method Including Wake Effects for Three-Dimensional Wing-Body Configurations. NASA TP-1910, 1981.

2. McLean, J. D.; and Randall, J. L.: Computer Program to Calculate Three-Dimensional Boundary Layer Flows over Wings with Wall Mass Transfer. NASA CR-3123, 1979.

3. Wai, J.; Baille, J.; and Yoshihara, H.: Calculations over Wings in the Boundary-Layer Limit. Boeing Aero TN D6-52894, Boeing Military Airplane Co., 1985.

4. Swafford, T. W.; and Whitfield, D. L.: Time-Dependent Solution of Three-Dimensional Compressible Turbulent Integral Boundary-Layer Equations. AIAA Journal, Vol. 23, No. 7, July, 1985.

5. Cebeci, T.; Kaups, K.; and Ramsey, J. A.: A General Method for Calculating Three-Dimensional Compressible Laminar and Turbulent Boundary Layers on Arbitary Wings. NASA CR-2777, 1977.

6. Matsuno, L.: A Vector-Orientated Finite-Difference Scheme for Calculating Three-Dimensional Compressible Laminar and Turbulent Boundary Layers on Practical Wing Configurations. AIAA Paper 81-1020, 1981.

7. Van Dalsem, W. R.; and Steger, J. L.: Using the Boundary-Layer Equations in Three-Dimensional Viscous Flow Simulation. Applications of Computational Fluid Dynamics in Aeronautics, Paper No. 24, AGARD CP 412, 1986.

8. Caughey, C. A.; and Jameson, A.: Recent Progess in Finite-Volume Calculations for Wing-Fuselage Combinations. AIAA Paper No. 79-1513, 1979.

9. Streett, C. L.; and Melson, N. D.: TAWFIVE: A User's Guide. NASA TM-84619, 1983.

10. Cebeci, T.: Calculation of Three-Dimensional Boundary Layers. I. Swept Infinite Cylinders and Small Cross Flow. AIAA Journal, Vol. 12, June 1974, pp. 779-786.

11. Woodson, S. H.; and DeJarnette, F. R.: A Three-Dimensional Boundary Layer Method for Flow over Delta Wings with Leading-Edge Separation. SAE Paper No. 851818, 1985.

12. Blottner, F. G.: Nonuniform Grid Method for Turbulent Boundary Layers. Lecture Notes in Physics, Vol. 35, 1975, pp. 91-97.

13. Woodson, S. H.: A Three-Dimensional Laminar Boundary Layer Method for Incompressible Flow over Delta Wings with Leading-Edge Separations. M.S. Thesis, N.C. State Univ., Raleigh, N.C., 1985.

14. Anderson, D. A.; Tannehill, J. C.; and Pletcher, R. H.: Computational Fluid Mechanics and Heat Transfer. McGraw-Hill, New York, 1984.

15. Raetz, G. S.: A Method of Calculating Three-Dimensional Laminar Boundary Layers of Steady Compressible Flows. Report No. NAI-58-73, Northrop Aircraft Inc., 1957.

16. Kitchens, C. W.; Gerber, N.; and Sedney, R.: Computational Implications of the Zone of Dependence Concept for Three-Dimensional Boundary Layers on a Spinning Body. Report No. 1774, Ballistic Research Labs, 1975.

17. Moore, F. K.: Displacement Effect of a Three-Dimensional Boundary Layer. NACA Report 1124, 1952.

18. Wang, K. C.: Boundary Layer over a Blunt Body at High Incidence with Open-Type of Separation. Proc. Roy. Soc., A340, 1974.

19. Cebeci, T.; Kattab, A. A.; and Stewartson, K.: Three-Dimensional Laminar Boundary Layers and the Ok of Accessibility. J. of Fluid Mech., Vol. 107, 1981.

20. Peake, D. J.; and Topak, M.: On Issues Concerning Flow Separation and Vortical Flows in Three Dimensions. NASA TM-84374, 1983.

21. Topak, M.; and Peake, D. J.: Topology of Three-Dimensional Separated Flows. Ann. Rev. Fluid Mech., Vol. 14, 1982.

22. Schmitt, V.; and Charpin, F.: Pressure Distributions on the ONERA M6 Wing at Transonic Mach Numbers. AGARD-AR-138, Chap. B-1, 1979.

23. Spaid, F. W.; and Roos, F. W.: An Experimental Study of the Turbulent Boundary Layer on a Transport Wing in Transonic Flow. AIAA Paper No. 83-1687, 1983.

24. Spaid, F. W.: Transonic Airfoil and Wing Flowfield Measurments. AIAA Paper No. 84-0100, 1984.

25. Clauser, F. H.: Turbulent Boundary Layers in Adverse Pressure Gradient. J. Aero. Sci., Vol. 21, 1954, pp. 91-108.

26. Spaid, F. W.: Comparisons Among Measured and Computed Boundary-Layer Properties on a Transport Wing. AIAA Paper No. 87-2555-CP, 1987.

27. Cebeci, T.; Chang, K. C.; and Clark, R. W.: Applications of Two- and Three-Dimensional Interactive Boundary-Layer Theory to Finite Wings with Flow Separation. AIAA Paper No. 87-0590, 1987.

28. Cebeci, T.: Problems and Opportunities with Three-Dimensional Boundary Layers. Three-Dimensional Boundary Layers, Paper No. 6, AGARD-R-719, 1984.

29. Cebeci, T.; and Smith, A. M. O.: Analysis of Turbulent Boundary Layers. Academic Press, New York, 1974.

30. Spiegel, M. R.: Vector Analysis. Schaum Publishing Co., New York, 1959.

APPENDIX A. DERIVATION OF THE UNIT VECTORS AND METRIC COEFFICIENTS

In order to write the governing boundary-layer equations in a body-orientated coordinate system, it is necessary to relate the curvilinear coordinates to a reference orthogonal coordinate system. This will yield expressions for the curvilinear unit vectors and metric coefficients. A constant-chord line (figure 1) is defined as,

$$\xi = \frac{\bar{x} - \bar{x}_{le}}{c} \tag{A1}$$

In general, the wing sweep and cross-sectional shape are functions of ξ and $\bar{y}$. It can be shown that the differential of eq. (A1), holding ξ = constant, yields,

$$\tan \Lambda = \tan \Lambda_{le} - \xi\Delta \tag{A2}$$

where,

$$\Delta = \tan \Lambda_{le} - \tan \Lambda_{te} \tag{A3}$$

The equation for the wing surface is given by,

$$\bar{F}(\bar{x},\bar{y},\bar{z}) = \bar{z} - c\bar{f}(\xi,\bar{y}) = 0 \tag{A4}$$

Therefore,

$$\nabla\bar{F} = \left[\frac{\partial\bar{F}}{\partial\bar{x}}\right] \hat{i} + \left[\frac{\partial\bar{F}}{\partial\bar{y}}\right] \hat{j} + \left[\frac{\partial\bar{F}}{\partial\bar{z}}\right] \hat{k}$$

$$= \left[-c \frac{\partial\bar{f}}{\partial\xi} \frac{\partial\xi}{\partial\bar{x}}\right] \hat{i} - \left[\bar{f} \frac{\partial c}{\partial\bar{y}} + c \left(\frac{\partial\bar{f}}{\partial\xi} \frac{\partial\xi}{\partial\bar{y}} + \frac{\partial\bar{f}}{\partial\bar{y}}\right)\right] \hat{j} + \hat{k}$$

$$= [- \tan \kappa] \hat{i} + \left[\bar{f}\Delta + \tan \Lambda \tan \kappa - c \frac{\partial\bar{f}}{\partial\bar{y}}\right] \hat{j} + \hat{k} \tag{A5}$$

and

$$|\nabla\bar{F}| = \sec\kappa \left\{1 + \left[\tan\Lambda \sin\kappa + \cos\kappa \left(\bar{f}\Delta - c\frac{\partial\bar{f}}{\partial\bar{y}}\right)\right]^2\right\}^{1/2} \tag{A6}$$

Define an angle Γ such that,

$$\tan\Gamma = \tan\Lambda \sin\kappa + \cos\kappa \left(\bar{f}\Delta - c\frac{\partial\bar{f}}{\partial\bar{y}}\right) \tag{A7}$$

Then a unit vector which is normal to the surface of the wing is defined by the equation,

$$\hat{e}_n = \frac{\nabla\bar{F}}{|\nabla\bar{F}|} = -\cos\Gamma \sin\kappa\, \hat{i} + \sin\Gamma\, \hat{j} + \cos\Gamma \cos\kappa\, \hat{k} \tag{A8}$$

Referring to figure 1, a streamwise unit vector which is orthogonal to $\hat{e}_n$ is defined by,

$$\hat{e}_s = \cos\kappa\, \hat{i} + \sin\kappa\, \hat{k} \tag{A9}$$

Next, define a unit vector $\hat{e}_{yo}$ which is tangent to an ξ = constant line in the $\bar{z} = 0$ plane (figure 2) by,

$$\hat{e}_{yo} = \sin\Lambda\, \hat{i} + \cos\Lambda\, \hat{j} \tag{A10}$$

Then a spanwise unit vector which is orthogonal to $\hat{e}_n$ with its component in the $\bar{z} = 0$ plane in the direction of $\hat{e}_{yo}$ may be defined by the relation,

$$\hat{e}_y \cdot \hat{e}_{yo} = \cos\Omega \tag{A11}$$

Thus,

$$\hat{e}_y = \cos\Omega\, \hat{e}_{yo} - \sin\Omega\, \hat{k}$$

$$= \cos\Omega \sin\Lambda\, \hat{i} + \cos\Omega \cos\Lambda\, \hat{j} - \sin\Omega\, \hat{k} \tag{A12}$$

Since $\hat{e}_y$ was defined to be normal to $\hat{e}_n$, their dot product must equal zero which yields,

$$\tan \Omega = \frac{\cos \Lambda \sin \Gamma - \sin \Lambda \cos \Gamma \sin \kappa}{\cos \Gamma \cos \kappa} \tag{A13}$$

Note that both $\hat{e}_s$ and $\hat{e}_y$ are perpendicular to $\hat{e}_n$. However, the coordinate system is nonorthogonal because the dot product of e_s and $\hat{e}_y$ is not zero and is given by,

$$\cos \Theta = \hat{e}_s \cdot \hat{e}_y = \cos \kappa \cos \Omega \, (\sin \Lambda - \tan \kappa \tan \Omega) \tag{A14}$$

The position vector of a point $(\bar{x},\bar{y},\bar{z})$ in Cartesian coordinates is given by,

$$\vec{R} = \bar{x}\,\hat{i} + \bar{y}\,\hat{j} + \bar{z}\,\hat{k} \tag{A15}$$

The same point may be represented in the curvilinear coordinate system by (s,y,n). However, since s and y vary along the wing it is more convenient to choose as independent variables (s_r,y_{le},n) where s_r refers to s along the root chord and y_{le} refers to y along the wing leading edge. Thus any point $(\bar{x},\bar{y},\bar{z})$ may be uniquely described by (s_r,y_{le},n). Then the differential of the position vector on the surface of the wing is given by,

$$\begin{aligned} d\vec{R} &= \left(\frac{\partial \bar{x}}{\partial s_r} ds_r + \frac{\partial \bar{x}}{\partial y_{le}} dy_{le}\right) \hat{i} + \left(\frac{\partial \bar{y}}{\partial s_r} ds_r + \frac{\partial \bar{y}}{\partial y_{le}} dy_{le}\right) \hat{j} \\ &\quad + \left(\frac{\partial \bar{z}}{\partial s_r} ds_r + \frac{\partial \bar{z}}{\partial y_{le}} dy_{le}\right) \hat{k} \\ &= h_1 \, ds_r \, \hat{e}_s + h_2 \, dy_{le} \, \hat{e}_y \end{aligned} \tag{A16}$$

where h_1 and h_2 are the metric coefficients which relate any point on the wing $(s,y,0)$ to the independent surface variables $(s_r,y_{le},0)$. From eq. (A16) one may obtain,

$$h_1 \hat{e}_s = \frac{\partial \bar{x}}{\partial s_r} \hat{i} + \frac{\partial \bar{y}}{\partial s_r} \hat{j} + \frac{\partial \bar{z}}{\partial s_r} \hat{k}$$

$$h_2 \hat{e}_y = \frac{\partial \bar{x}}{\partial y_{le}} \hat{i} + \frac{\partial \bar{y}}{\partial y_{le}} \hat{j} + \frac{\partial \bar{z}}{\partial y_{le}} \hat{k} \tag{A17}$$

Performing the indicated differentiation gives,

$$\frac{\partial \bar{x}}{\partial s_r} = \left(\frac{c}{c_r}\right) \cos \kappa_r \tag{A18a}$$

$$\frac{\partial \bar{y}}{\partial s_r} = 0 \tag{A18b}$$

$$\frac{\partial \bar{z}}{\partial s_r} = \left(\frac{c}{c_r}\right) \cos \kappa_r \tan \kappa \tag{A18c}$$

and

$$\frac{\partial \bar{x}}{\partial y_{le}} = \tan\Lambda \cos\Omega_{le} \cos\Lambda_{le} \tag{A19a}$$

$$\frac{\partial \bar{y}}{\partial y_{le}} = \cos\Omega_{le} \cos\Lambda_{le} \tag{A19b}$$

$$\frac{\partial \bar{z}}{\partial y_{le}} = -\tan\Omega \cos\Omega_{le} \cos\Lambda_{le}/\cos\Lambda \tag{A19c}$$

Thus, the solution of eq. (A17) yields the metric coefficients as,

$$h_1 = \frac{c \cos \kappa_r}{c_r \cos \kappa} \tag{A20}$$

$$h_2 = \frac{\cos \Lambda_{le} \cos \Omega_{le}}{\cos \Lambda \cos \Omega} \tag{A21}$$

APPENDIX B. DERIVATION OF THE NONORTHOGONAL BOUNDARY-LAYER EQUATIONS

With expressions for the unit vectors and metric coefficients in the curvilinear coordinate system the conservation equations may be derived. The velocity vector is given by,

$$\vec{V} = u\,\hat{e}_s + v\,\hat{e}_y + w\,\hat{e}_n \tag{B1}$$

where u, v, and w are the velocity components streamwise, spanwise and normal to the wing surface, respectively. The substantial derivative of the velocity vector is therefore,

$$\frac{D\vec{V}}{Dt} = \frac{Du}{Dt}\hat{e}_s + \frac{Dv}{Dt}\hat{e}_y + \frac{Dw}{Dt}\hat{e}_n + u\frac{D\hat{e}_s}{Dt} + v\frac{D\hat{e}_y}{Dt} + w\frac{D\hat{e}_n}{Dt} \tag{B2}$$

Thus, in order to calculate the derivative of the velocity vector, one must first determine the derivatives of the curvilinear unit vectors. To obtain a unit vector along any coordinate line, differentiate the position vector (eq. (A15)) with respect to the particular coordinate and divide by its magnitude. Thus,

$$\hat{e}_s = \frac{\partial\vec{R}}{\partial s_r} \Big/ \left|\frac{\partial\vec{R}}{\partial s_r}\right|$$

$$= \frac{\partial\vec{R}}{\partial s_r} \Big/ \left[\left(\frac{\partial\bar{x}}{\partial s_r}\right)^2 + \left(\frac{\partial\bar{y}}{\partial s_r}\right)^2 + \left(\frac{\partial\bar{z}}{\partial s_r}\right)^2\right]^{1/2}$$

$$= \frac{\partial\vec{R}}{\partial s_r} \Big/ h_1 \tag{B3a}$$

In a similar manner,

$$\hat{e}_y = \frac{\partial\vec{R}}{\partial y_{1e}} \Big/ h_2 \tag{B3b}$$

Differentiating eq. (B3a) with respect to y_{1e} and eq. (B3b) with respect to s_r yields,

$$\frac{\partial^2 \vec{R}}{\partial y_{1e}\, \partial s_r} = \frac{\partial}{\partial y_{1e}} (h_1\, \hat{e}_s) = \frac{\partial}{\partial s_r} (h_2\, \hat{e}_y) = \frac{\partial^2 \vec{R}}{\partial s_r\, \partial y_{1e}} \tag{B4}$$

Then it follows that,

$$\frac{\partial h_1}{\partial y_{1e}}\, \hat{e}_s + h_1 \frac{\partial \hat{e}_s}{\partial y_{1e}} = \frac{\partial h_2}{\partial s_r}\, \hat{e}_y + h_2 \frac{\partial \hat{e}_y}{\partial s_r} \tag{B5}$$

Taking the dot product of each term in eq. (B5) with $\hat{e}_s$ gives,

$$\frac{\partial \hat{e}_y}{\partial s_r} \cdot \hat{e}_s = \frac{1}{h_2} \left(\frac{\partial h_1}{\partial y_{1e}} - \cos \Theta \frac{\partial h_2}{\partial s_r}\right) \tag{B6}$$

where eq. (A14) was used for the dot product of $\hat{e}_s$ and $\hat{e}_y$. Next, take the dot product of each term in eq. (B5) with e_y to get,

$$\frac{\partial \hat{e}_s}{\partial y_{1e}} \cdot \hat{e}_y = \frac{1}{h_1} \left(\frac{\partial h_2}{\partial s_r} - \cos \Theta \frac{\partial h_1}{\partial y_{1e}}\right) \tag{B7}$$

Differentiating eq. (A14) with respect to s_r yields,

$$\hat{e}_s \cdot \frac{\partial \hat{e}_y}{\partial s_r} + \hat{e}_y \cdot \frac{\partial \hat{e}_s}{\partial s_r} = - \sin \Theta \frac{\partial \Theta}{\partial s_r} \tag{B8}$$

and using eq. (B6) in eq. (B8) one may obtain,

$$\frac{\partial \hat{e}_s}{\partial s_r} \cdot \hat{e}_y = \frac{1}{h_2} \left[\frac{\partial}{\partial s_r} (h_2 \cos \Theta) - \frac{\partial h_1}{\partial y_{1e}}\right] \tag{B9}$$

Similarily differentiating eq. (A14) with respect to y_{1e} gives,

$$\hat{e}_s \cdot \frac{\partial \hat{e}_y}{\partial y_{1e}} + \hat{e}_y \cdot \frac{\partial \hat{e}_s}{\partial y_{1e}} = - \sin \Theta \frac{\partial \Theta}{\partial y_{1e}} \tag{B10}$$

and using eq. (B7) in eq. (B10) one may obtain,

$$\frac{\partial \hat{e}_y}{\partial y_{le}} \cdot \hat{e}_s = \frac{1}{h_1} \left[\frac{\partial}{\partial y_{le}} (h_1 \cos \Theta) - \frac{\partial h_2}{\partial s_r} \right] \tag{B11}$$

Now consider the derivative of $\hat{e}_s$ with respect to some argument, q ($q = s_r, y_{le}, n$) which may be written as,

$$\frac{\partial \hat{e}_s}{\partial q} = a_s \hat{e}_s + b_s \hat{e}_y + c_s \hat{e}_n \tag{B12}$$

Taking the dot product of each term in the above with $\hat{e}_s$ and then taking the dot product of each term with e_y will yield expressions for a_s and b_s which are,

$$b_s = \csc^2 \Theta \left(\frac{\partial \hat{e}_s}{\partial q} \cdot \hat{e}_y \right)$$

$$a_s = - \cot \Theta \csc \Theta \left(\frac{\partial \hat{e}_s}{\partial q} \cdot \hat{e}_y \right) \tag{B13}$$

Substituting eq. (B13) into eq. (B12) yields,

$$\frac{\partial \hat{e}_s}{\partial q} = \left(\frac{\partial \hat{e}_s}{\partial q} \cdot \hat{e}_y \right) \left[-\cot \Theta \csc \Theta \hat{e}_s + \csc^2 \Theta \hat{e}_y \right] + c_s \hat{e}_n \tag{B14}$$

Following a similar procedure for the derivative of $\hat{e}_y$ it can be shown that,

$$\frac{\partial \hat{e}_y}{\partial q} = \left(\frac{\partial \hat{e}_y}{\partial q} \cdot \hat{e}_s \right) \left[\csc^2 \Theta \hat{e}_s - \cot \Theta \csc \Theta \hat{e}_y \right] + c_y \hat{e}_n \tag{B15}$$

The terms c_s and c_y only contribute to the normal momentum equation and their explicit values need not be determined under the thin boundary-layer assumption. Using eqs. (B7) and (B9) in eq. (B14) yields,

$$\frac{\partial \hat{e}_s}{\partial s_r} = \frac{1}{h_2}\left[\frac{\partial}{\partial s_r}(h_2 \cos\theta) - \frac{\partial h_1}{\partial y_{le}}\right](-\cot\theta \csc\theta\, \hat{e}_s + \csc^2\theta\, \hat{e}_y)$$

$$+ c_s\, \hat{e}_n \tag{B16a}$$

$$\frac{\partial \hat{e}_s}{\partial y_{le}} = \frac{1}{h_1}\left[\frac{\partial h_2}{\partial s_r} - \cos\theta \frac{\partial h_1}{\partial y_{le}}\right](-\cot\theta \csc\theta\, \hat{e}_s + \csc^2\theta\, \hat{e}_y)$$

$$+ c_s\, \hat{e}_n \tag{B16b}$$

and using eqs. (B6) and (B11) in eq. (B15) gives,

$$\frac{\partial \hat{e}_y}{\partial s_r} = \frac{1}{h_2}\left[\frac{\partial h_1}{\partial y_{le}} - \cos\theta \frac{\partial h_2}{\partial s_r}\right](\csc^2\theta\, \hat{e}_s - \cot\theta \csc\theta\, \hat{e}_y)$$

$$+ c_y\, \hat{e}_n \tag{B17a}$$

$$\frac{\partial \hat{e}_y}{\partial y_{le}} = \frac{1}{h_1}\left[\frac{\partial}{\partial y_{le}}(h_1 \cos\theta) - \frac{\partial h_2}{\partial s_r}\right](\csc^2\theta\, \hat{e}_s - \cot\theta \csc\theta\, \hat{e}_y)$$

$$+ c_y\, \hat{e}_n \tag{B17b}$$

The substantial derivative for steady flow in the curvilinear coordinate system is given by,

$$\frac{D}{Dt} = u\frac{\partial}{\partial s} + v\frac{\partial}{\partial y} + w\frac{\partial}{\partial n}$$

$$= \frac{u}{h_1}\frac{\partial}{\partial s_r} + \frac{v}{h_2}\frac{\partial}{\partial y_{le}} + w\frac{\partial}{\partial n} \tag{B18}$$

Substituting eqs. (B16) and (B17) into the above yields,

$$\frac{D\hat{e}_s}{Dt} = K_1 u (-\cot\theta \hat{e}_s + \csc\theta \hat{e}_y) + [c_s(\frac{u}{h_1} + \frac{v}{h_2}) + w \frac{\partial \hat{e}_s}{\partial n}] \hat{e}_n$$

$$+ \frac{v}{h_1 h_2 \sin\theta} [\frac{\partial h_2}{\partial s_r} - \cos\theta \frac{\partial h_1}{\partial y_{1e}}](-\cot\theta \hat{e}_s + \csc\theta \hat{e}_y) \quad \text{(B19)}$$

and

$$\frac{D\hat{e}_y}{Dt} = \frac{u}{h_1 h_2 \sin\theta} [\frac{\partial h_1}{\partial y_{1e}} - \cos\theta \frac{\partial h_2}{\partial s_r}] (\csc\theta \hat{e}_s - \cot\theta \hat{e}_y)$$

$$+ K_2 v (\csc\theta \hat{e}_s - \cot\theta \hat{e}_y) + [c_y (\frac{u}{h_1} + \frac{v}{h_2}) + w \frac{\partial \hat{e}_y}{\partial n}] \hat{e}_n \quad \text{(B20)}$$

where K_1 and K_2 are the geodesic curvatures of the curves y_{1e} = constant, and s_r = constant, respectively, and are given by,

$$K_1 = \frac{1}{h_1 h_2 \sin\theta} [\frac{\partial}{\partial s_r} (h_2 \cos\theta) - \frac{\partial h_1}{\partial y_{1e}}] \quad \text{(B21)}$$

$$K_2 = \frac{1}{h_1 h_2 \sin\theta} [\frac{\partial}{\partial y_{1e}} (h_1 \cos\theta) - \frac{\partial h_2}{\partial s_r}] \quad \text{(B22)}$$

Using eqs. (B19) and (B20) in eq. (B2) gives the substantial derivative of the velocity vector as,

$$\frac{D\vec{V}}{Dt} = [\frac{Du}{Dt} - K_1 \cot\theta u^2 + K_2 \csc\theta v^2 + K_{12} uv] \hat{e}_s$$

$$+ [\frac{Dv}{Dt} - K_2 \cot\theta v^2 + K_1 \csc\theta u^2 + K_{21} uv] \hat{e}_y$$

$$+ [\frac{Dw}{Dt} + w (\frac{\partial \hat{e}_s}{\partial n} + \frac{\partial \hat{e}_y}{\partial n}) + (c_s + c_y)(\frac{u}{h_1} + \frac{v}{h_2})] \hat{e}_n$$

$$+ w \frac{D\hat{e}_n}{Dt} \quad \text{(B23)}$$

where the parameters K_{12} and K_{21} are given by,

$$K_{12} = \frac{1}{h_1 h_2 \sin^2\Theta}\left[\frac{\partial h_1}{\partial y_{1e}}(1 + \cos^2\Theta) - 2\cos\Theta\frac{\partial h_2}{\partial s_r}\right] \tag{B24}$$

$$K_{21} = \frac{1}{h_1 h_2 \sin^2\Theta}\left[\frac{\partial h_2}{\partial s_r}(1 + \cos^2\Theta) - 2\cos\Theta\frac{\partial h_1}{\partial y_{1e}}\right] \tag{B25}$$

Next, consider the gradient of a scalar, p, which may be written as,

$$\nabla p = p_s \hat{e}_s + p_y \hat{e}_y + p_n \hat{e}_n \tag{B26}$$

The differential of a scalar is given by,

$$dp = \nabla p \cdot d\vec{R} \tag{B27}$$

where the differential of the position vector is,

$$d\vec{R} = h_1\, ds_r\, \hat{e}_s + h_2\, dy_{1e}\, \hat{e}_y + dn\, \hat{e}_n \tag{B28}$$

Using eqs. (B26) and (B28) in eq. (B27) yields,

$$dp = (p_s h_1 + p_y h_1 \cos\Theta)\, ds_r + (p_s h_2 \cos\Theta + p_y h_2)\, dy_{1e} + p_n dn \tag{B29}$$

However, dp may also be written as,

$$dp = \frac{\partial p}{\partial s_r} ds_r + \frac{\partial p}{\partial y_{1e}} dy_{1e} + \frac{\partial p}{\partial n} dn \tag{B30}$$

Equating eqs. (B29) and (B30) and solving for p_s and p_y gives,

$$p_s = \frac{\csc^2\Theta}{h_1}\frac{\partial p}{\partial s_r} - \frac{\cot\Theta\,\csc\Theta}{h_2}\frac{\partial p}{\partial y_{1e}} \tag{B31a}$$

$$p_y = \frac{\csc^2\Theta}{h_2}\frac{\partial p}{\partial y_{1e}} - \frac{\cot\Theta\,\csc\Theta}{h_1}\frac{\partial p}{\partial s_r} \tag{B31b}$$

With eq. (B31), eq. (B26) becomes,

$$\nabla p = \left[\frac{\csc^2\Theta}{h_1}\frac{\partial p}{\delta s_r} - \frac{\cot\Theta\ \csc\Theta}{h_2}\frac{\partial p}{\delta y_{le}}\right]\hat{e}_s$$

$$+ \left[\frac{\csc^2\Theta}{h_2}\ \frac{\partial p}{\delta y_{le}} - \frac{\cot\Theta\ \csc\Theta}{h_1}\frac{\partial p}{\delta s_r}\right]\hat{e}_y + \frac{\partial p}{\partial n}\hat{e}_n \qquad \text{(B32)}$$

The steady Navier-Stokes and Energy equations written in tensor notation [14] are (neglecting body forces),

$$\rho\frac{D\vec{V}}{Dt} = -\nabla p + \frac{\partial \tau_{ij}}{\partial x_j}, \qquad i,j,k = 1,2,3 \qquad \text{(B33)}$$

$$\frac{\partial}{\partial x_j}\left[\rho u_j H - \frac{\mu}{Pr}\frac{\partial}{\partial x_j}\left(H - \frac{u_T^2}{2}\right) - u_i\ \tau_{ij}\right] = 0 \qquad \text{(B34)}$$

where H is the total enthalpy, μ is the dynamic viscosity coefficient, Pr is the Prandtl number, u_T is the magnitude of the total velocity,

$$u_T^2 = u^2 + v^2 + 2\ uv\ \cos\Theta \qquad \text{(B35)}$$

and τ_{ij} is the stress tensor which is given by,

$$\tau_{ij} = \mu\left[\left(\frac{\partial u_i}{\partial x_j} + \frac{\partial u_j}{\partial x_i}\right) - \frac{2}{3}\delta_{ij}\frac{\partial u_k}{\partial x_k}\right] \qquad \text{(B36)}$$

The boundary-layer assumption is that the boundary layer consists of a thin viscous layer very close to the surface of the wing [14,29]. Therefore the variation of the pressure and the unit vectors across the boundary layer are assumed to be negligible. However, since the velocity components range from the inviscid values at the outer edge of the boundary layer down to zero at the wing surface, the velocity gradients normal to the wing are much larger than those parallel to the surface. Thus, in the viscous and heat-conduction terms, only the normal derivatives are retained. This produces a parabolic set of equations which may be solved by a streamwise marching procedure. Substituting eqs. (B23) and (B32) in eq. (B33) yields for the streamwise momentum equation,

$$\frac{\rho u}{h_1}\frac{\partial u}{\delta s_r} + \frac{\rho v}{h_2}\frac{\partial u}{\delta y_{le}} + \rho w\frac{\partial u}{\partial n} - \rho K_1\cot\Theta\ u^2 + \rho K_2\ \csc\Theta\ v^2$$

$$+ \rho K_{12} uv = - \frac{\csc^2\Theta}{h_1} \frac{\partial p}{\partial s_r} + \frac{\cot\Theta \csc\Theta}{h_2} \frac{\partial p}{\partial y_{le}} + \frac{\partial}{\partial n} \left(\mu \frac{\partial u}{\partial n}\right) \tag{B37}$$

and for the spanwise momentum equation,

$$\frac{\rho u}{h_1} \frac{\partial v}{\partial s_r} + \frac{\rho v}{h_2} \frac{\partial v}{\partial y_{le}} + \rho w \frac{\partial v}{\partial n} - \rho K_2 \cot\Theta\, v^2 + \rho K_1 \csc\Theta\, u^2$$

$$+ \rho K_{21} uv = - \frac{\csc^2\Theta}{h_2} \frac{\partial p}{\partial y_{le}} + \frac{\cot\Theta \csc\Theta}{h_1} \frac{\partial p}{\partial s_r} + \frac{\partial}{\partial n} \left(\mu \frac{\partial v}{\partial n}\right) \tag{B38}$$

Using eq. (B18) in eq. (B34) gives the energy equation as,

$$\frac{\rho u}{h_1} \frac{\partial H}{\partial s_r} + \frac{\rho v}{h_2} \frac{\partial H}{\partial y_{le}} + \rho w \frac{\partial H}{\partial n} = \frac{\partial}{\partial n} \left[\frac{\mu}{Pr} \frac{\partial H}{\partial n} + \mu \left(1 - \frac{1}{Pr}\right) \frac{\partial}{\partial n} \left(\frac{u_T^2}{2}\right)\right] \tag{B39}$$

Now consider a line element, $d\ell$, which in the tensor notation [30] is given by,

$$d\ell^2 = \sum_{i=1}^{3} \sum_{j=1}^{3} g_{ij}\, dx_i\, dx_j \tag{B40}$$

The quantities g_{ij} are the components of a covariant tensor of rank two called the fundamental tensor. The line element may also be written as,

$$d\ell^2 = d\vec{R} \cdot d\vec{R} = h_1^2\, ds_r^2 + h_2^2\, dy_{le}^2 + 2h_1h_2 \cos\Theta\, ds_r\, dy_{le} + dn^2 \tag{B41}$$

Comparison of eqs. (B40) and (B41) gives the elements of g_{ij},

$$g_{ij} = \begin{bmatrix} h_1^2 & h_1h_2\cos\Theta & 0 \\ h_1h_2\cos\Theta & h_2^2 & 0 \\ 0 & 0 & 1 \end{bmatrix} \tag{B42}$$

Therefore, g_{ij} is a symmetric tensor whose determinant is given by,

$$|g| = h_1^2 h_2^2 \sin^2\theta \tag{B43}$$

The divergence of a vector $\vec{V}$, in a general coordinate system is given in the tensor notation [30] as,

$$\nabla \cdot \vec{V} = \frac{1}{\sqrt{g}} \frac{\partial}{\partial x_i} [\sqrt{g}\, V^i] \quad , \qquad i = 1,2,3 \tag{B44}$$

where V^i is the contravariant velocity vector,

$$V^i = V_i / \sqrt{g_{ii}} = \left[\frac{u}{h_1} \quad \frac{v}{h_2} \quad w\right]^T \tag{B45}$$

With eqs. (B44) and (B45) the steady continuity equation may be derived,

$$\nabla \cdot (\rho \vec{V}) = 0$$

$$\frac{\partial}{\partial x_i} [\sqrt{g}\, \rho\, V^i] = 0$$

$$\frac{\partial}{\partial s_r} (\rho u h_2 \sin\theta) + \frac{\partial}{\partial y_{le}} (\rho v h_1 \sin\theta) + \frac{\partial}{\partial n} (\rho w h_1 h_2 \sin\theta) = 0 \tag{B46}$$

Equations (B46), (B37), (B38), and (B39) are the governing nonorthogonal boundary-layer equations for a laminar, compressible flow. To obtain the governing turbulent equations, the flow variables are defined as the sum of an average plus a fluctuating quantity and then substituted back into the original equations which are then time averaged [14]. However, the magnitude of the fluctuating flow variables is small compared to the average values, and under the boundary-layer approximation, only the fluctuating quantities which are multiplied by the normal velocity component need to be retained. This is because across the boundary layer, the average of the normal velocity component is of the same order of magnitude as its fluctuating component [14, 29]. Therefore a mass averaged normal velocity component is defined as,

$$\overline{\rho w} = \rho w + \overline{\rho' w'} \tag{B47}$$

and the governing equations become for a turbulent flow:

continuity equation,

$$\frac{\partial}{\partial s_r} (\rho u h_2 \sin\theta) + \frac{\partial}{\partial y_{le}} (\rho v h_1 \sin\theta) + \frac{\partial}{\partial n} (\overline{\rho w}\, h_1 h_2 \sin\theta) = 0 \tag{B48}$$

streamwise momentum equation,

$$\frac{\rho u}{h_1}\frac{\partial u}{\partial s_r} + \frac{\rho v}{h_2}\frac{\partial u}{\partial y_{1e}} + \overline{\rho w}\frac{\partial u}{\partial n} - \rho K_1 \cot\Theta\, u^2 + \rho K_2 \csc\Theta\, v^2$$

$$+ \rho K_{12}\, uv = \rho_e \left[\frac{u_e}{h_1}\frac{\partial u_e}{\partial s_r} + \frac{v_e}{h_2}\frac{\partial u_e}{\partial y_{1e}} - K_1 \cot\Theta\, u_e^2\right.$$

$$\left. + K_2 \csc\Theta\, v_e^2 + K_{12}\, u_e\, v_e\right] + \frac{\partial}{\partial n}\left(\mu\frac{\partial u}{\partial n} - \rho\,\overline{u'w'}\right) \qquad \text{(B49)}$$

spanwise momentum equation,

$$\frac{\rho u}{h_1}\frac{\partial v}{\partial s_r} + \frac{\rho v}{h_2}\frac{\partial v}{\partial y_{1e}} + \overline{\rho w}\frac{\partial v}{\partial n} - \rho K_2 \cot\Theta\, v^2 + \rho K_1 \csc\Theta\, u^2$$

$$+ \rho K_{21} uv = \rho_e \left[\frac{u_e}{h_1}\frac{\partial v_e}{\partial s_r} + \frac{v_e}{h_2}\frac{\partial v_e}{\partial y_{1e}} - K_2 \cot\Theta\, v_e^2\right.$$

$$\left. + K_1 \csc\Theta\, u_e^2 + K_{21} u_e v_e\right] + \frac{\partial}{\partial n}\left(\mu\frac{\partial v}{\partial n} - \rho\,\overline{v'w'}\right) \qquad \text{(B50)}$$

energy equation,

$$\frac{\rho u}{h_1}\frac{\partial H}{\partial s_r} + \frac{\rho v}{h_2}\frac{\partial H}{\partial y_{1e}} + \overline{\rho w}\frac{\partial H}{\partial n}$$

$$= \frac{\partial}{\partial n}\left[\frac{\mu}{Pr}\frac{\partial H}{\partial n} + \mu\left(1 - \frac{1}{Pr}\right)\frac{\partial}{\partial n}\left(\frac{u_T^2}{2}\right) - \rho\,\overline{w'H'}\right] \qquad \text{(B51)}$$

In eqs. (B49) and (B50) the pressure gradient terms have been replaced with their equivalent velocity gradient terms by applying eqs. (B37) and (B38) at the edge of the boundary layer.

APPENDIX C. COEFFICIENTS OF THE TRANSFORMED EQUATIONS

The coefficients for the three-dimensional boundary-layer equations in transformed variables are given below. The flow variables without an i subscript are evaluated at (i) for the predictor step and at (i + 1/2) for the corrector step. The parameter N has the value of one at the predictor step and two at the corrector step. The terms b_m, d_m, and e_m are defined by,

$$b_m = \begin{bmatrix} b_{m1} & b_{m3} \\ b_{m2} & b_{m4} \end{bmatrix} , \quad dm = \begin{bmatrix} d_{m1} & d_{m3} \\ d_{m2} & m_{m4} \end{bmatrix} , \quad e_m = \begin{bmatrix} e_{m1} \\ e_{m2} \end{bmatrix} \tag{C1}$$

The coefficients for the momentum equations are given by,

$$a_m = b_{j,k-1/2} / \Delta\eta_{k-1}$$

$$c_m = b_{j,k+1/2} / \Delta\eta_k$$

$$b_{m1} = b_{m4} = a_m + c_m + (\Delta\eta_k + \Delta\eta_{k-1})\, m_{10}\, F_{j,k} / \Delta s_r$$

$$b_{m2} = b_{m3} = 0 \tag{C2}$$

$$d_{m1} = - m_{10}\, (F_{j,k+1} - F_{j,k-1}) / \Delta s_r$$

$$d_{m2} = - m_{10}\, (G_{j,k+1} - G_{j,k-1}) / \Delta s_r$$

$$d_{m3} = d_{m4} = 0 \tag{C3}$$

$$t_1 = \frac{N}{2}\, \sigma_{2_{j,k}}$$

$$t_2 = \frac{N}{4} m_7 \, (g_{j+1,k} - g_{j-1,k})/\Delta y_{le}$$

$$t_3 = - m_{10} \, f_{i,j,k}/\Delta s_r$$

$$t_{4a} = (t_1 + t_2 + t_3) * (F_{j,k+1} - F_{j,k-1})$$

$$t_{4b} = (t_1 + t_2 + t_3) * (G_{j,k+1} - G_{j,k-1})$$

$$t_{5a} = m_{10} \, (\Delta\eta_k + \Delta\eta_{k-1}) \, F_{j,k} \, F_{i,j,k}/\Delta s_r$$

$$t_{5b} = m_{10} \, (\Delta\eta_k + \Delta\eta_{k-1}) \, F_{j,k} \, G_{i,j,k}/\Delta s_r$$

$$t_{6a} = - \frac{N}{4} m_7 \, (\Delta\eta_k + \Delta\eta_{k-1}) \, G_{j,k} \, (F_{j+1,k} - F_{j-1,k})/\Delta y_{le}$$

$$t_{6b} = - \frac{N}{4} m_7 \, (\Delta\eta_k + \Delta\eta_{k-1}) \, G_{j,k} \, (G_{j+1,k} - G_{j-1,k})/\Delta y_{le}$$

$$t_{7a} = m_2 \, F^2_{j,k} + m_5 \, F_{j,k} \, G_{j,k} + m_8 \, G^2_{j,k} - m_{11} \, c_{2_{j,k}}$$

$$t_{7b} = m_9 \, F^2_{j,k} + m_4 \, F_{j,k} \, G_{j,k} + m_3 \, G^2_{j,k} - m_{12} \, c_{2_{j,k}} \qquad \text{(C4)}$$

$$e_{m1} = t_{4a} + t_{5a} + t_{6a} - \frac{N}{2} \, (\Delta\eta_k + \Delta\eta_{k-1}) \, t_{7a}$$

$$e_{m2} = t_{4b} + t_{5b} + t_{6b} - \frac{N}{2} \, (\Delta\eta_k + \Delta\eta_{k-1}) \, t_{7b} \qquad \text{(C5)}$$

At the corrector step the e_m vector has the additional terms,

$$e_{m1} = e_{m1} + c_m (F_{i,j,k+1} - F_{i,j,k}) - a_m (F_{i,j,k} - F_{i,j,k-1})$$

$$e_{m2} = e_{m2} + c_m (G_{i,j,k+1} - G_{i,j,k}) - a_m (G_{i,j,k} - G_{i,j,k-1}) \qquad (C6)$$

For the solution of the energy equation the term $\hat{f}_{j,k}$ means $f_{i+1/2,j,k}$ at the predictor step and $f_{i+1,j,k}$ at the corrector step. The energy equation coefficients are defined by,

$$a_e = \sigma 1_{j,k-1/2} \; / \; \Delta\eta_{k-1}$$

$$c_e = \sigma 1_{j,k+1/2} \; / \; \Delta\eta_k$$

$$b_e = a_e + c_e + m_{10} (\Delta\eta_k + \Delta\eta_{k-1}) F_{j,k}/\Delta s_r \qquad (C7)$$

$$t_8 = \frac{N}{2} \sigma 2_{j,k}$$

$$t_9 = m_{10} (\hat{f}_{j,k} - f_{i,j,k})/\Delta s_r$$

$$t_{10} = \frac{N}{4} m_7 (g_{j+1,k} - g_{j-1,k})/\Delta y_{1e}$$

$$t_{11} = (t_8 + t_9 + t_{10}) * (E_{j,k+1} - E_{j,k-1})$$

$$t_{12} = -\frac{N}{4} m_7 G_{j,k} (\Delta\eta_k + \Delta\eta_{k-1})(E_{j+1,k} - E_{j-1,k})/\Delta y_{1e}$$

$$t_{13} = N \sigma 4_{j,k-1/2} (F_{j,k-1} - F_{j,k})/\Delta\eta_{k-1}$$

$$t_{14} = N \sigma 4_{j,k+1/2} (F_{j,k+1} - F_{j,k})/\Delta\eta_k$$

$$t_{15} = N\,\sigma_{5_{j,k-1/2}}\,(G_{j,k-1} - G_{j,k})/\Delta\eta_{k-1}$$

$$t_{16} = N\,\sigma_{5_{j,k+1/2}}\,(G_{j,k+1} - G_{j,k})/\Delta\eta_{k}$$

$$t_{17} = m_{10}\,(\Delta\eta_k + \Delta\eta_{k-1})\,F_{j,k}\,E_{i,j,k} \,/\, \Delta s_r \qquad (C8)$$

$$d_e = t_{11} + t_{12} + t_{13} + t_{14} + t_{15} + t_{16} + t_{17} \qquad (C9)$$

and at the corrector step d_e has the additional terms,

$$d_e = d_e + c_e\,(E_{i,j,k+1} - E_{i,j,k}) - a_e\,(E_{i,j,k} - E_{i,j,k-1}) \qquad (C10)$$

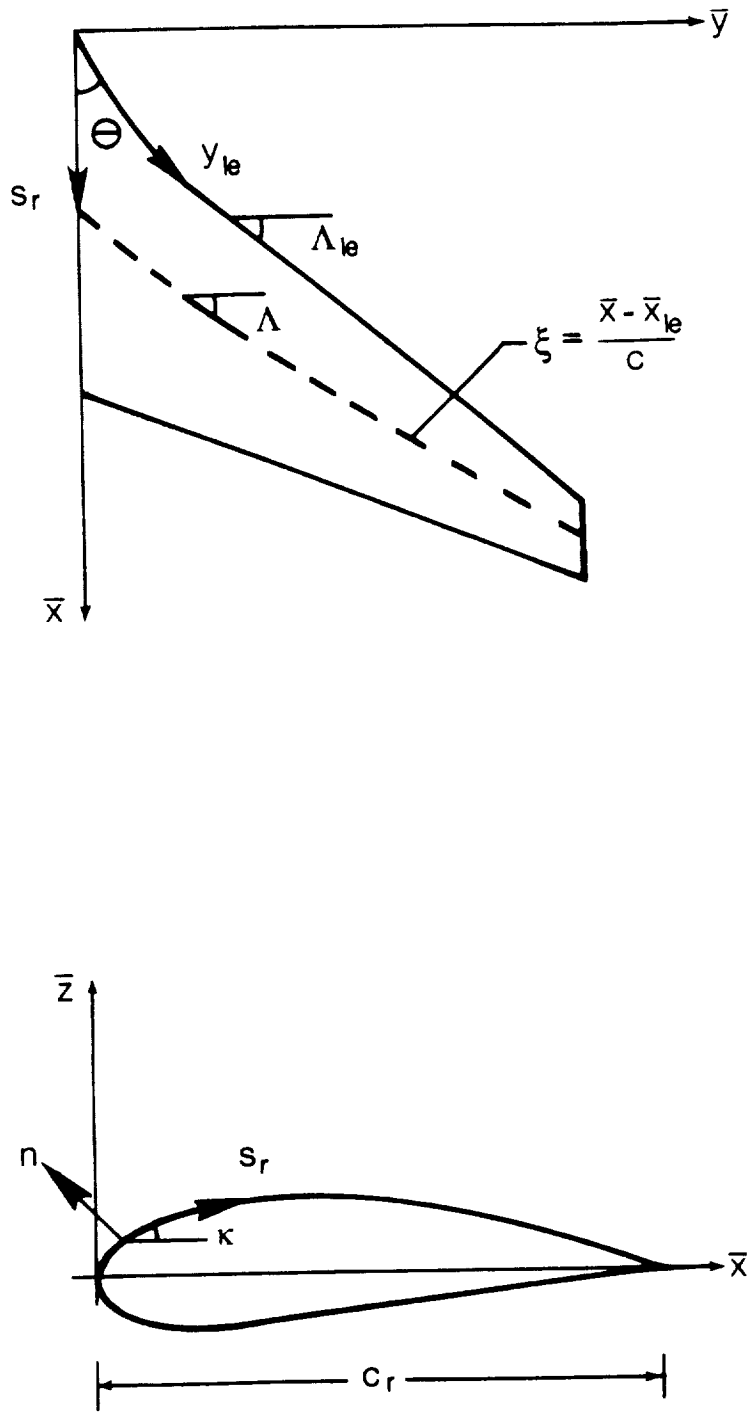

Figure 1. Nonorthogonal curvilinear coordinate system.

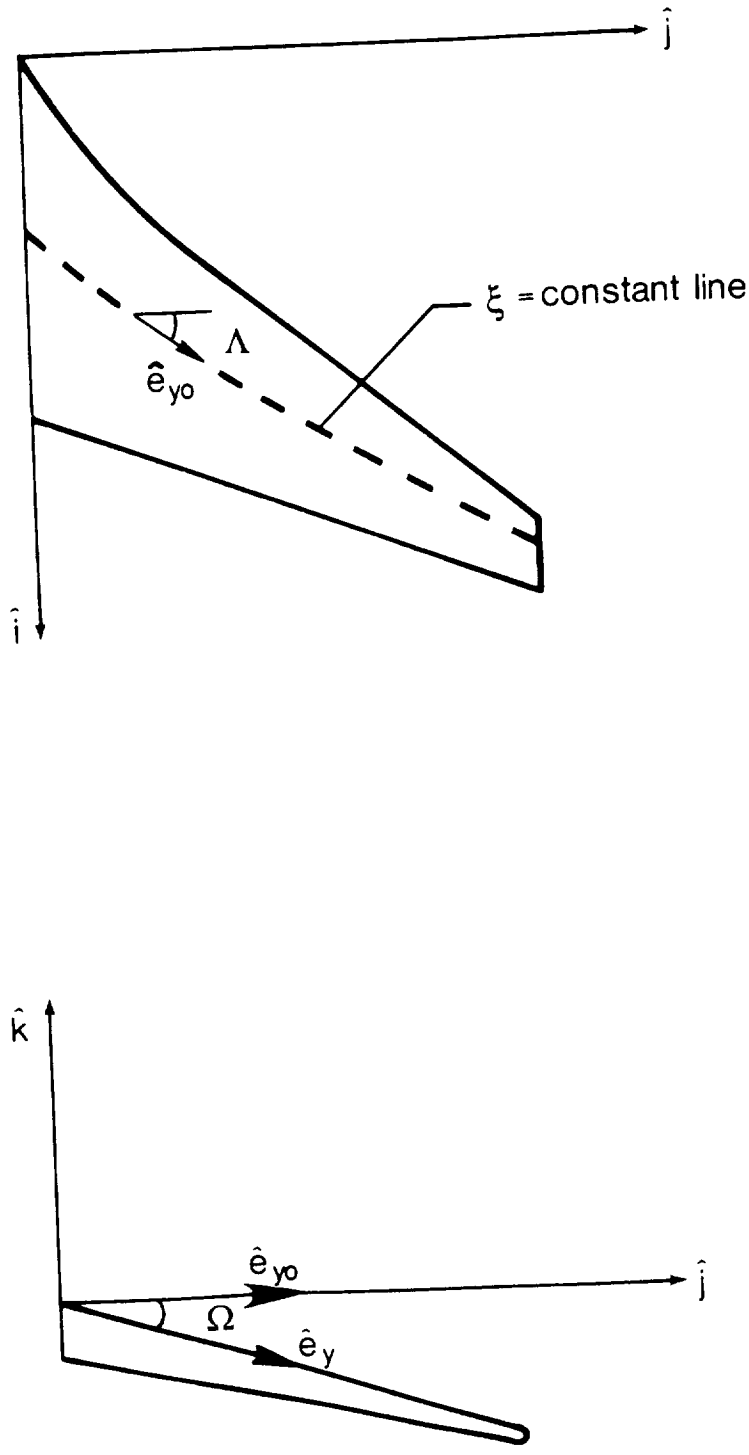

Figure 2. Definition of the spanwise unit vector.

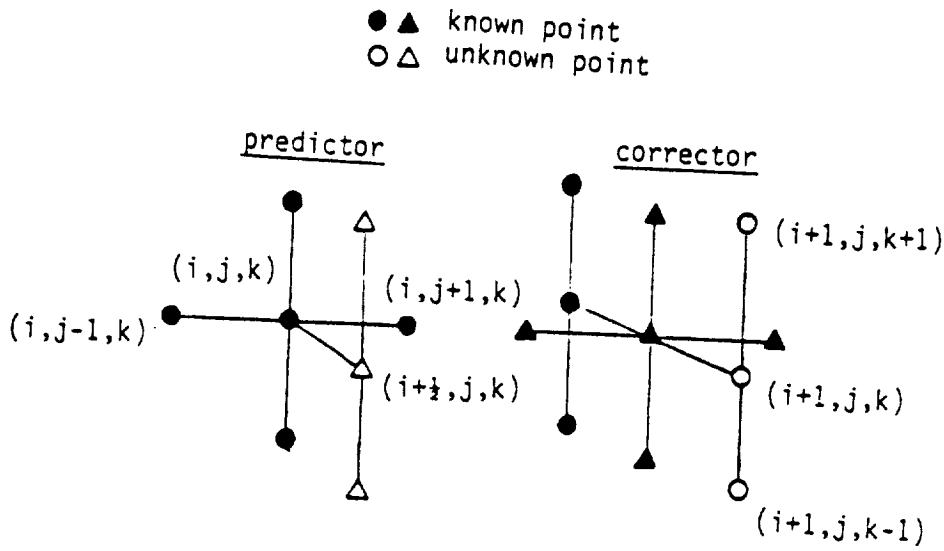

Figure 3. Finite-difference cell.

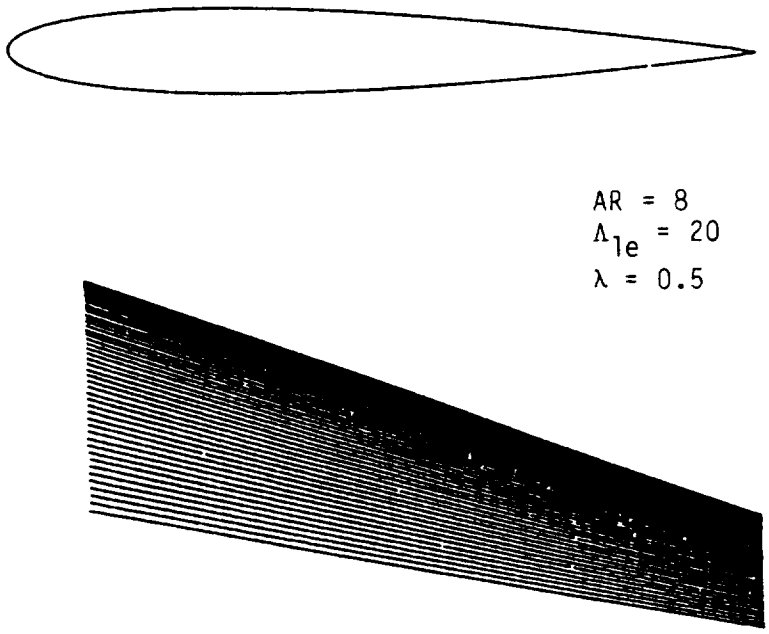

Figure 4. Planform of the NACA 0012 wing.

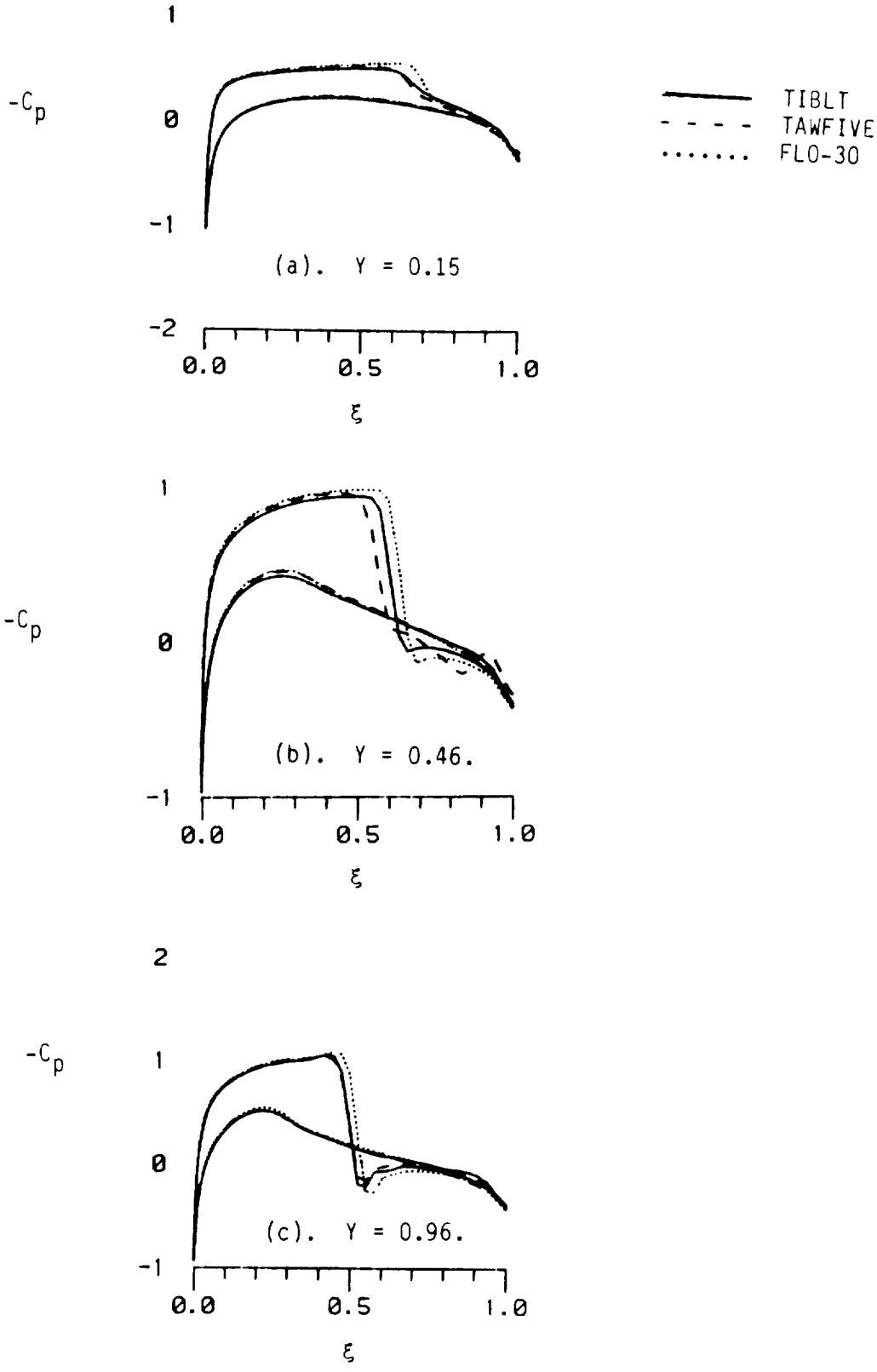

Figure 5. Pressure coefficient distributions for the NACA 0012 wing, $M_\infty = 0.85$.

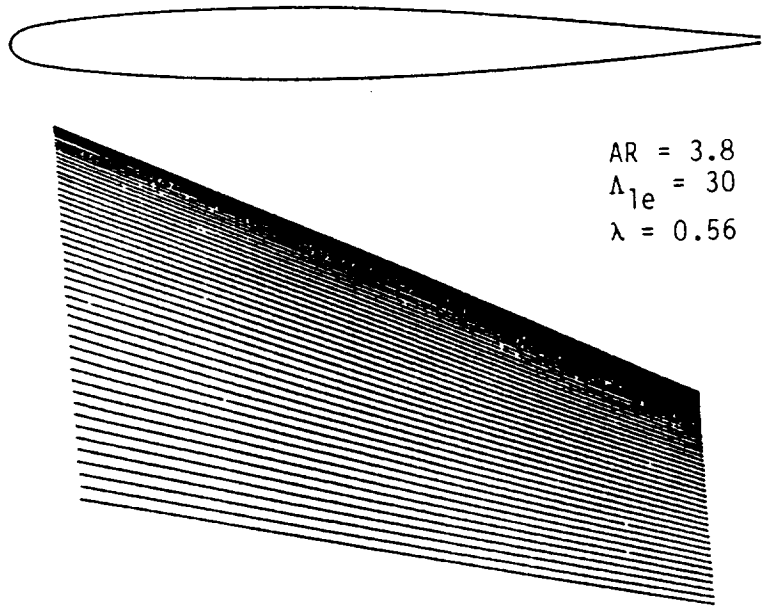

Figure 6. Planform of the ONERA M6 wing (ref. 22).

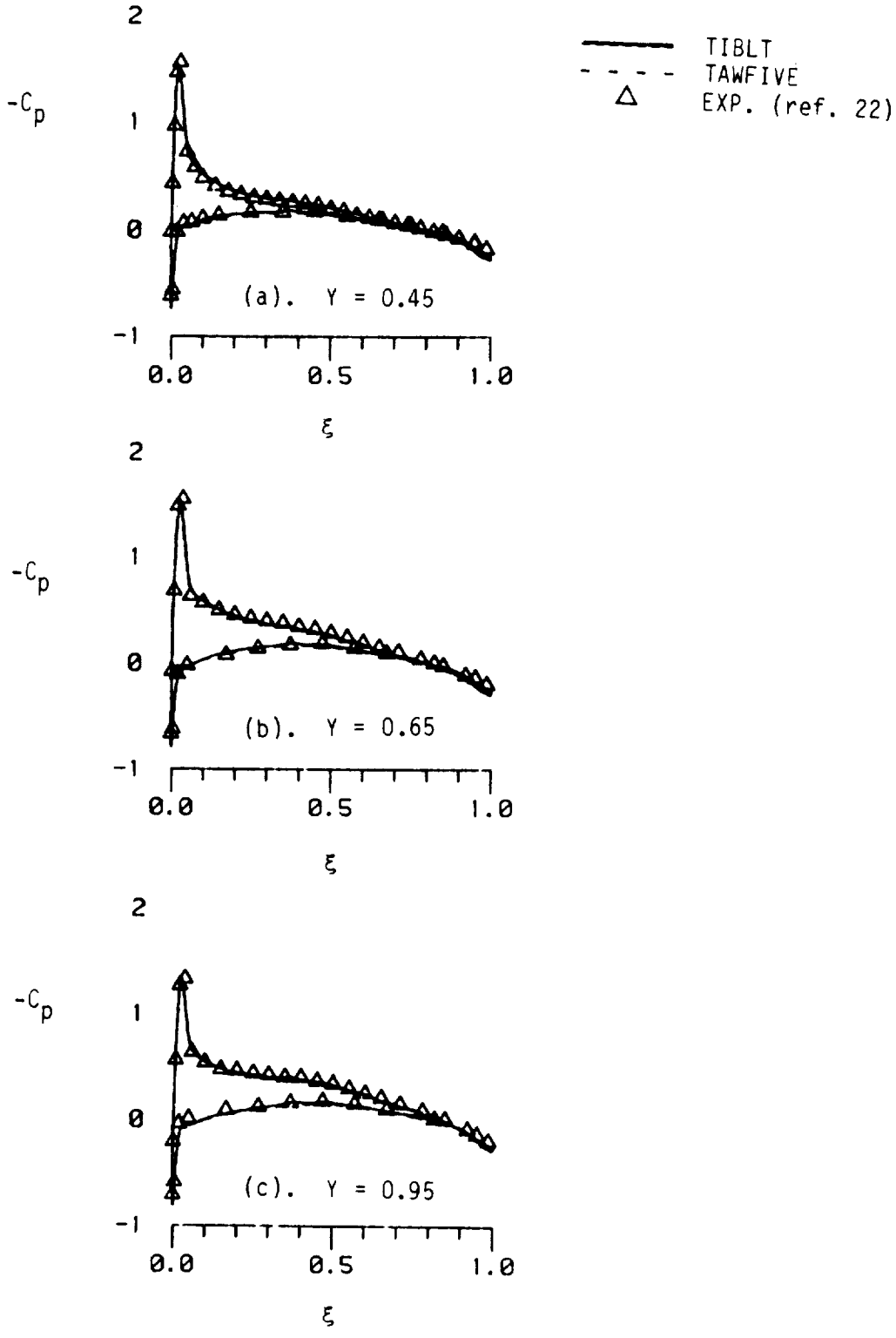

Figure 7. Pressure coefficient distribution for the M6 wing, M_∞ = 0.699.

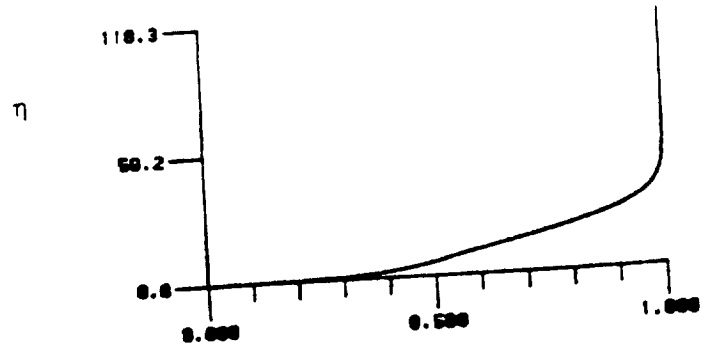

F

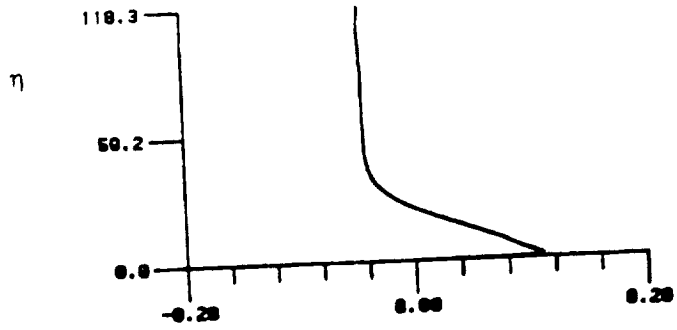

G

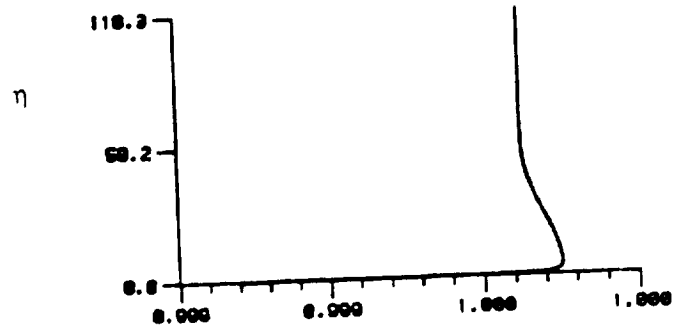

E

Figure 8. Velocity and total enthalpy profiles at ξ = 1.0 and Y = 0.46 for the M6 wing, M_∞ = 0.699.

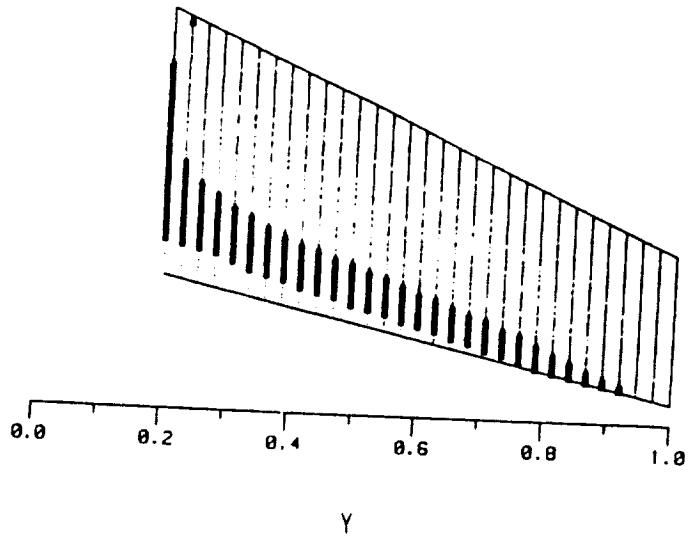

Figure 9. Locations of velocity crossover on the upper surface of the M6 wing, $M_\infty = 0.699$.

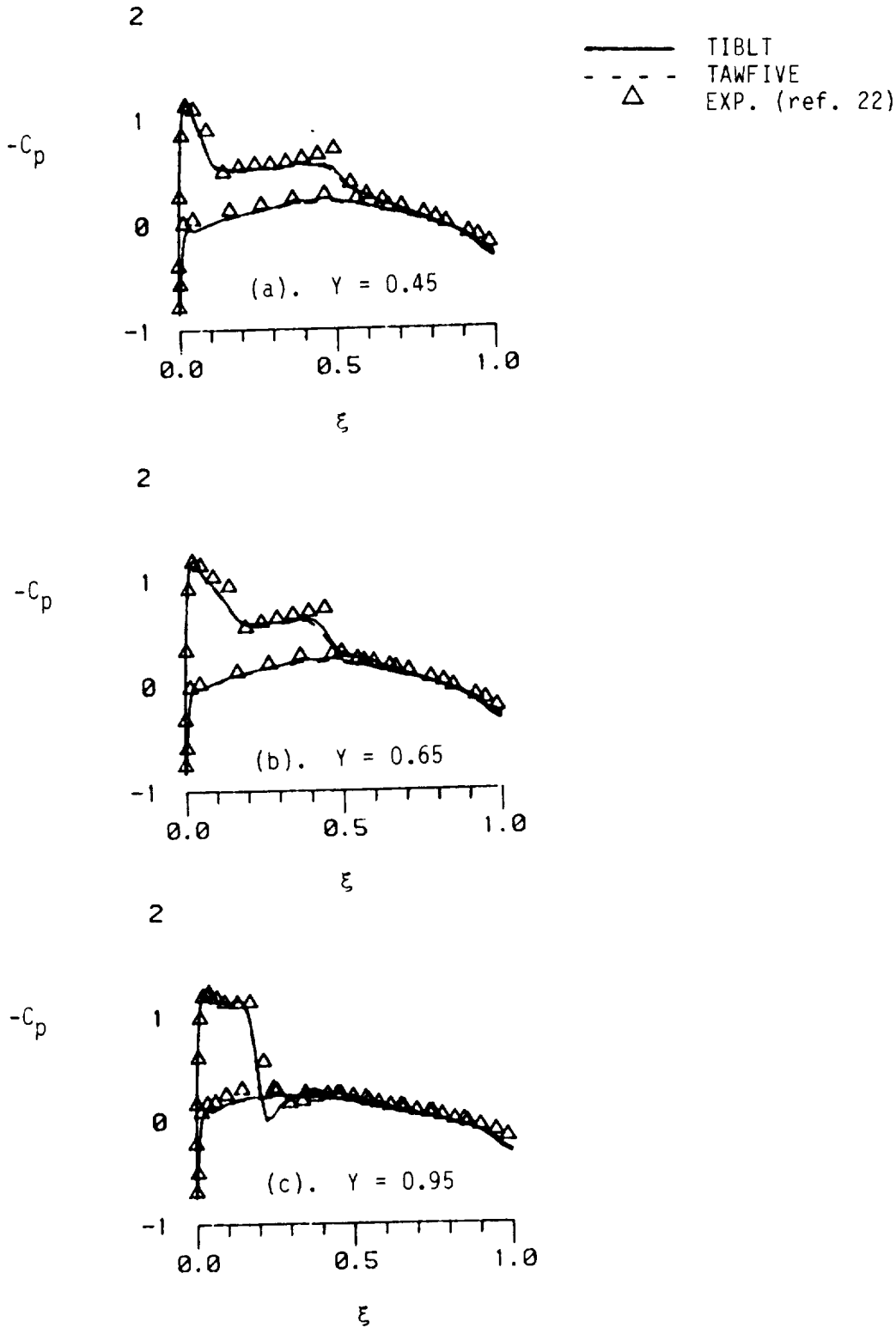

Figure 10. Pressure coefficient distribution for the M6 wing, M_∞ = 0.84.

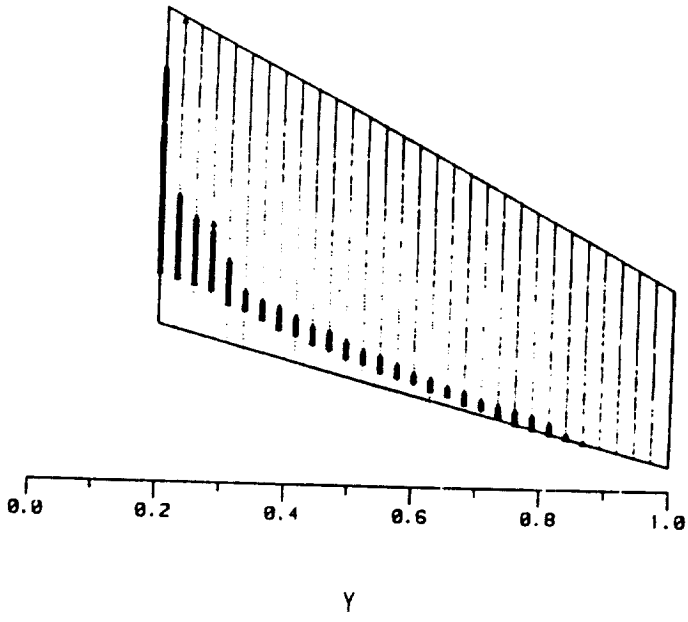

Figure 11. Locations of velocity crossover on the upper surface of the M6 wing, $M_\infty = 0.84$.

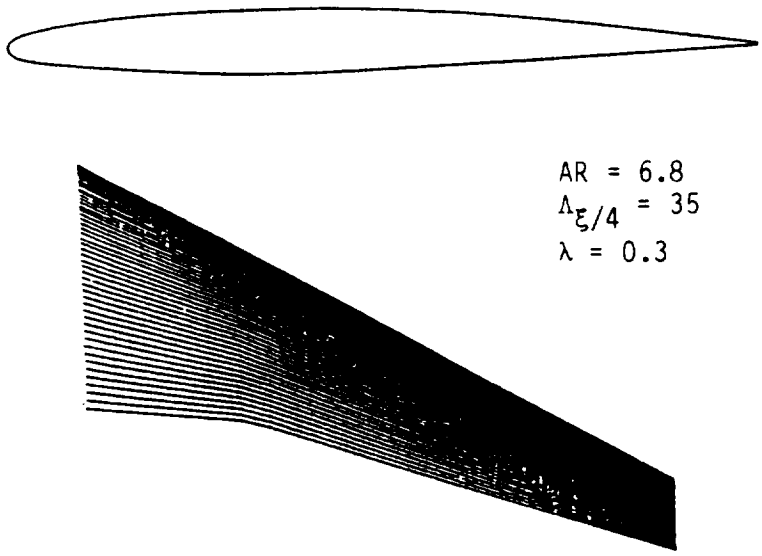

Figure 12. Planform of the DAC wing (ref. 23).

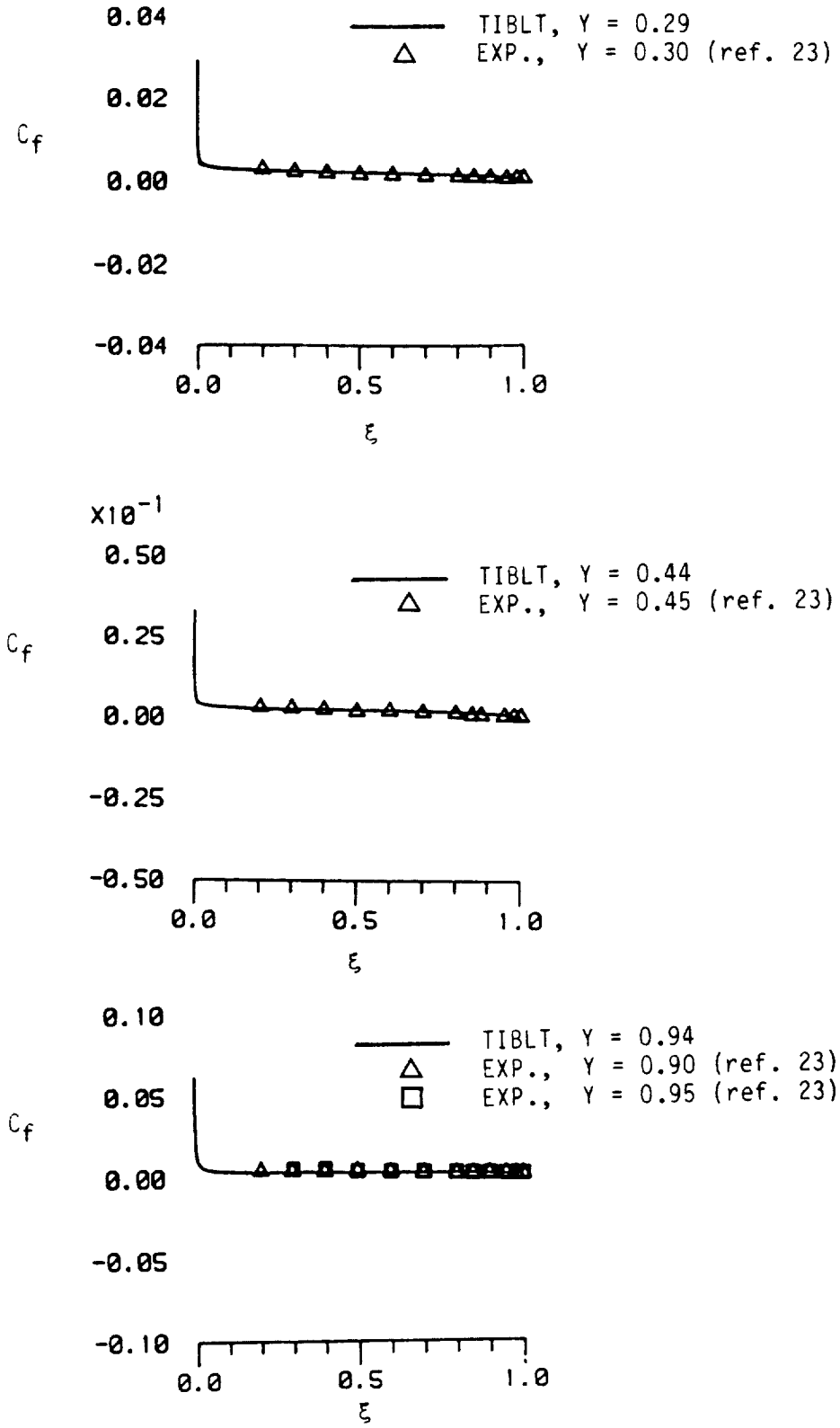

Figure 15. Skin-friction coefficient distribution for the DAC wing, M_∞ = 0.5.

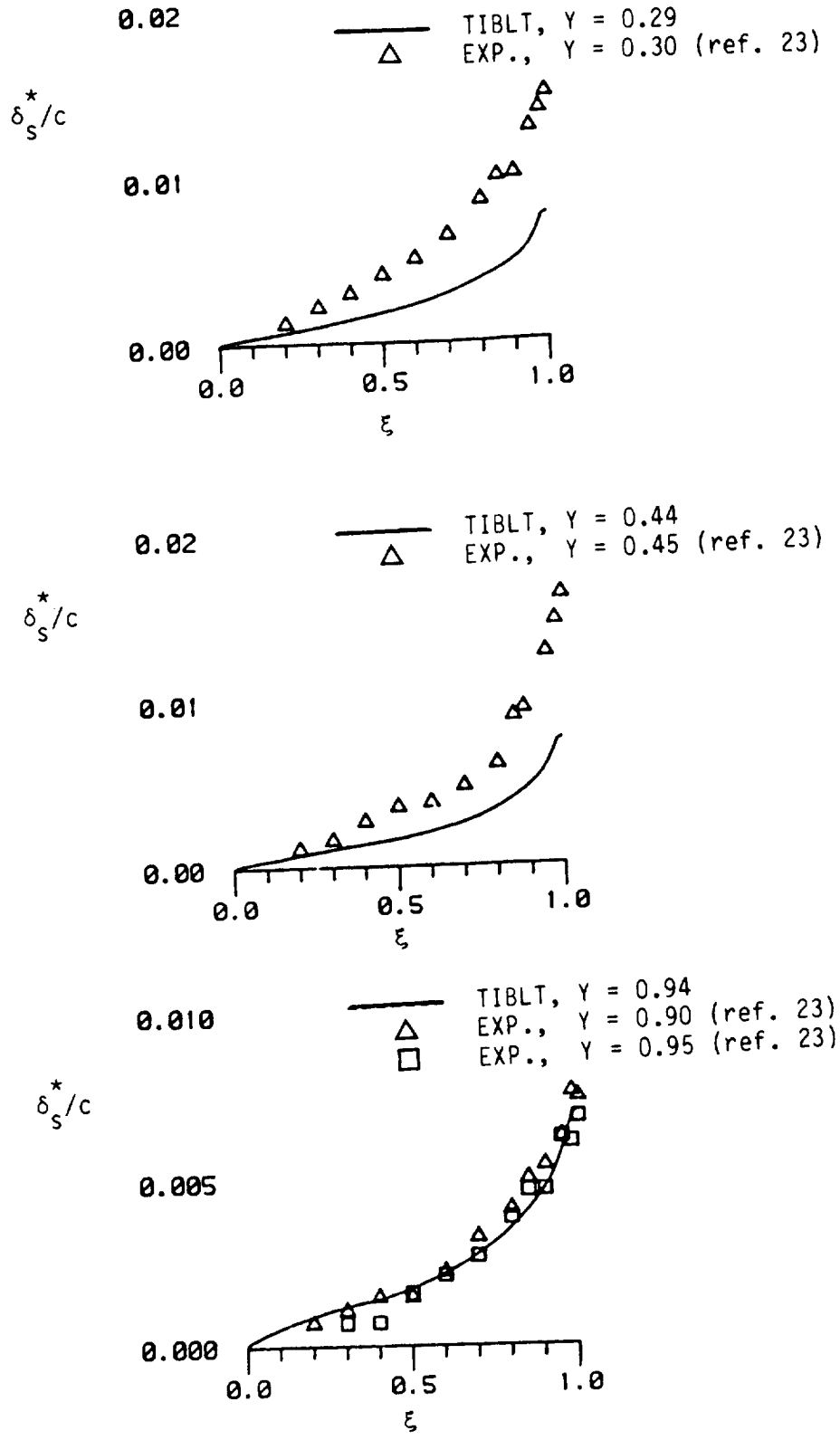

Figure 16. Streamwise velocity integral thickness distribution for the DAC wing, $M_\infty = 0.5$.

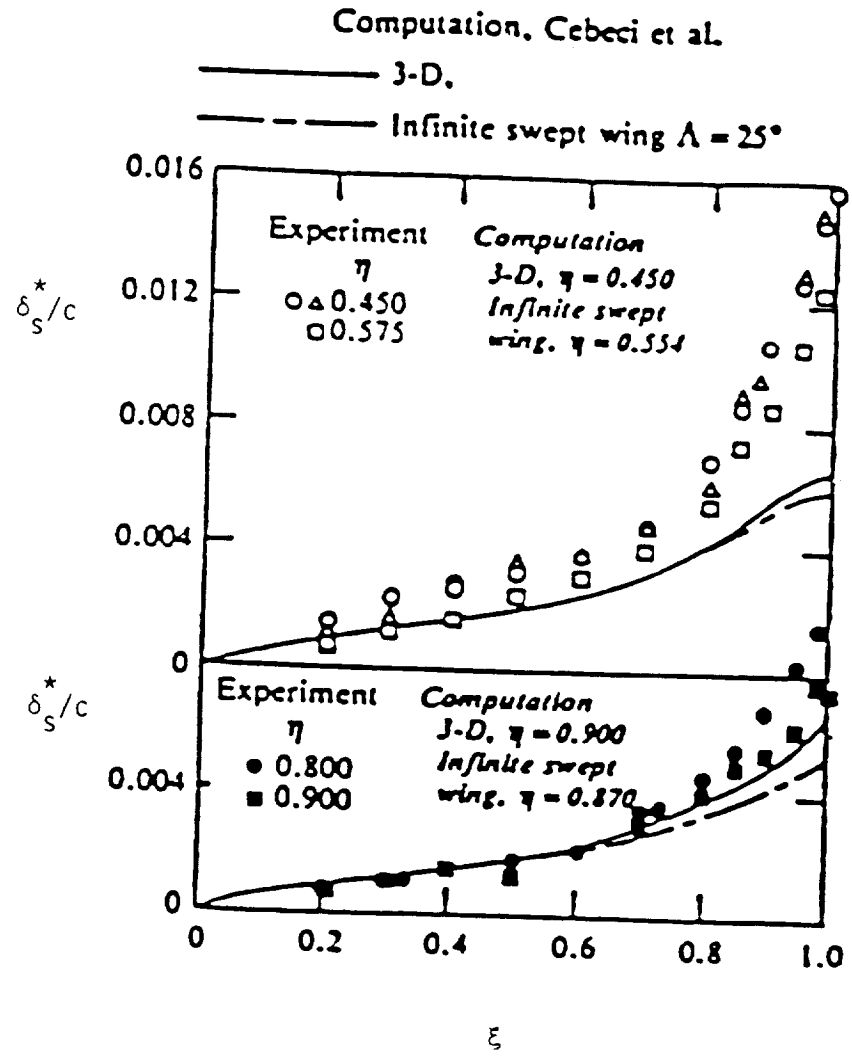

Figure 17. Streamwise velocity integral thickness distribution for the DAC wing, M_∞ = 0.5 (from ref. 26).

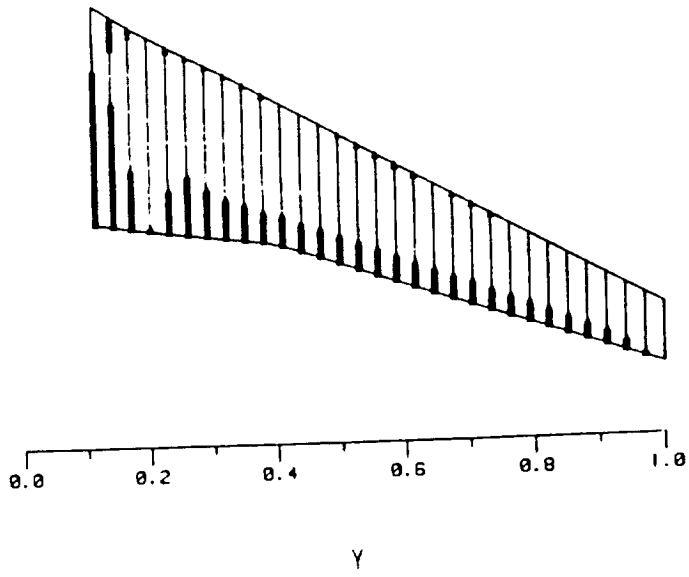

Figure 18. Locations of velocity crossover on the upper surface of the DAC wing, $M_\infty = 0.5$.

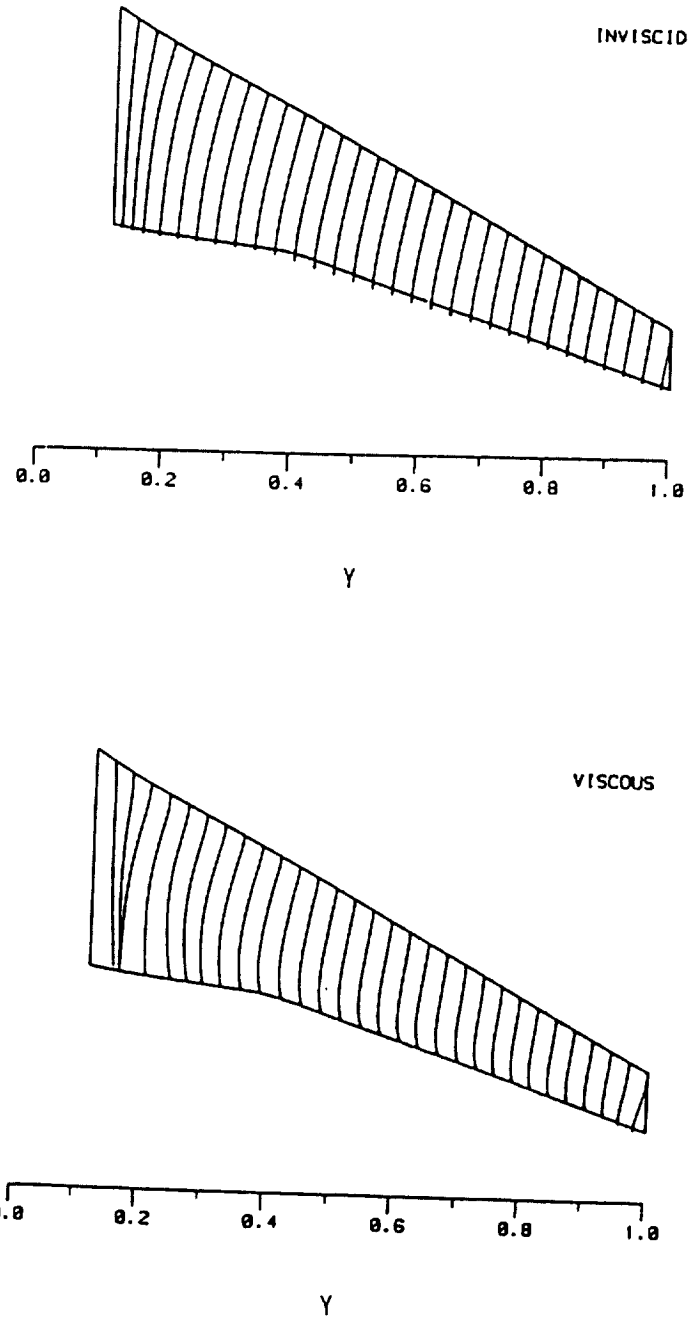

Figure 19.- Inviscid and viscous streamlines for the DAC wing, $M_\infty = 0.5$.

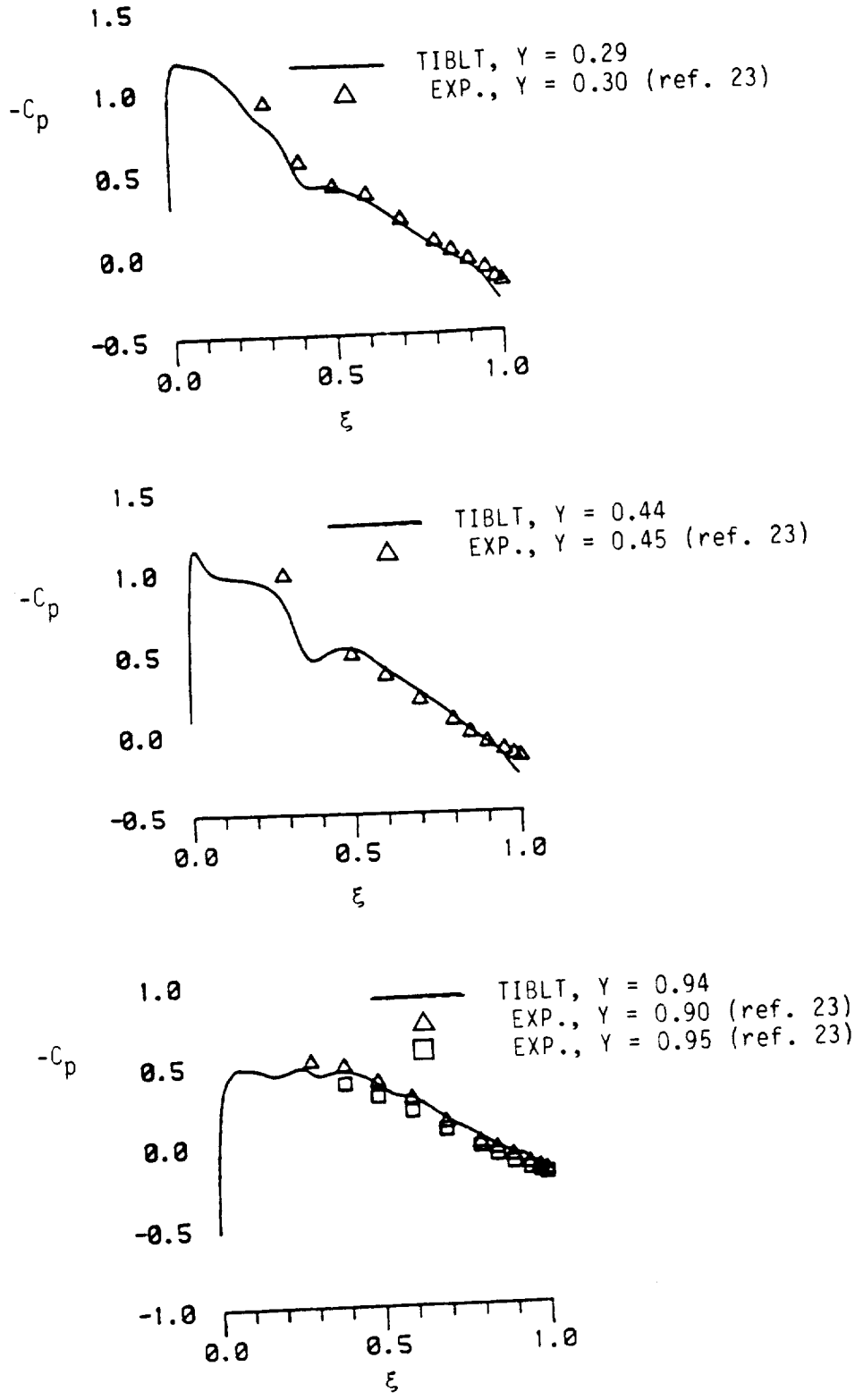

Figure 20. Upper surface pressure coefficient distribution for the DAC wing, $M_\infty = 0.825$.

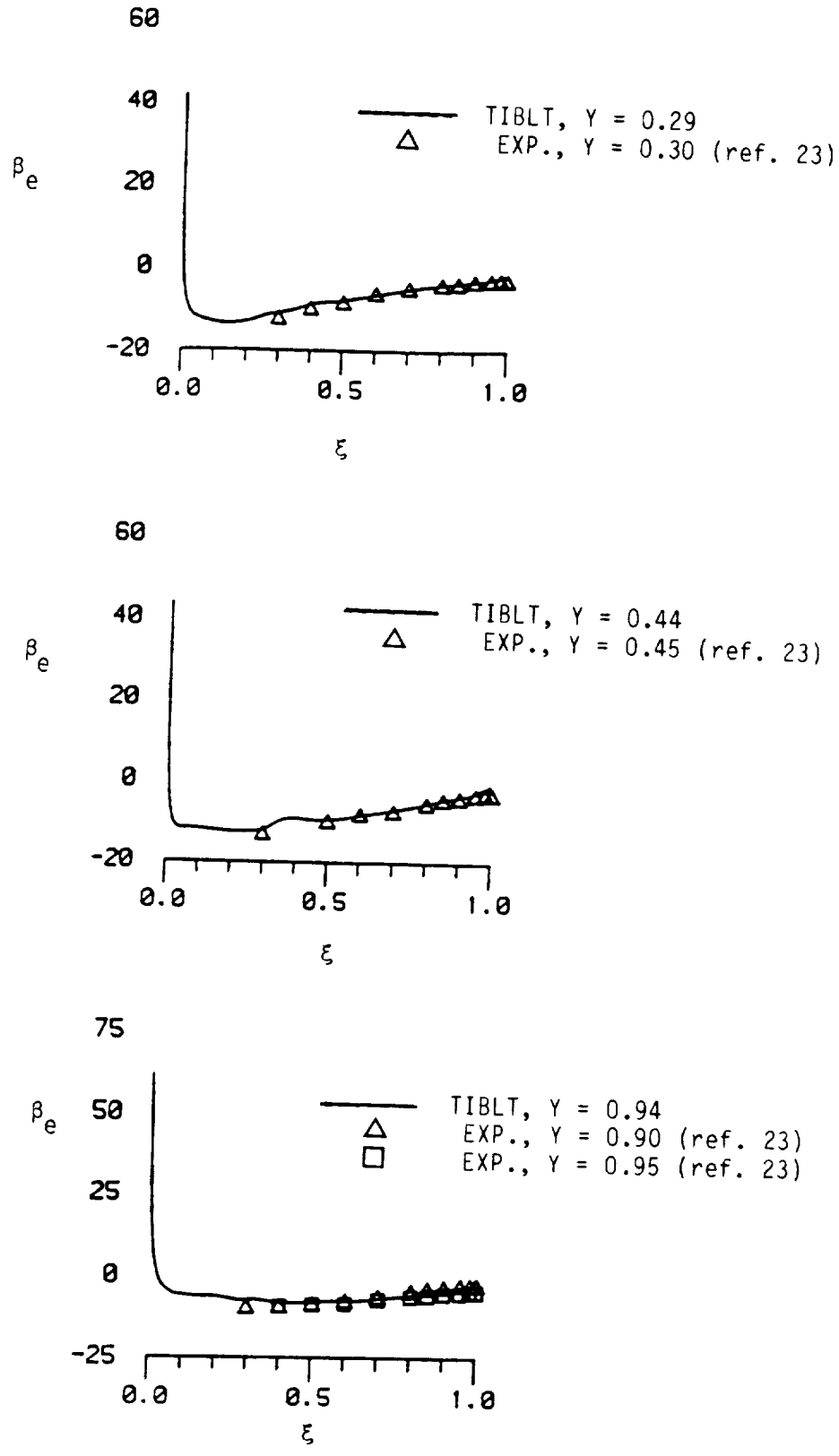

Figure 21. Inviscid flow-direction angle for the DAC wing, $M_\infty = 0.825$.

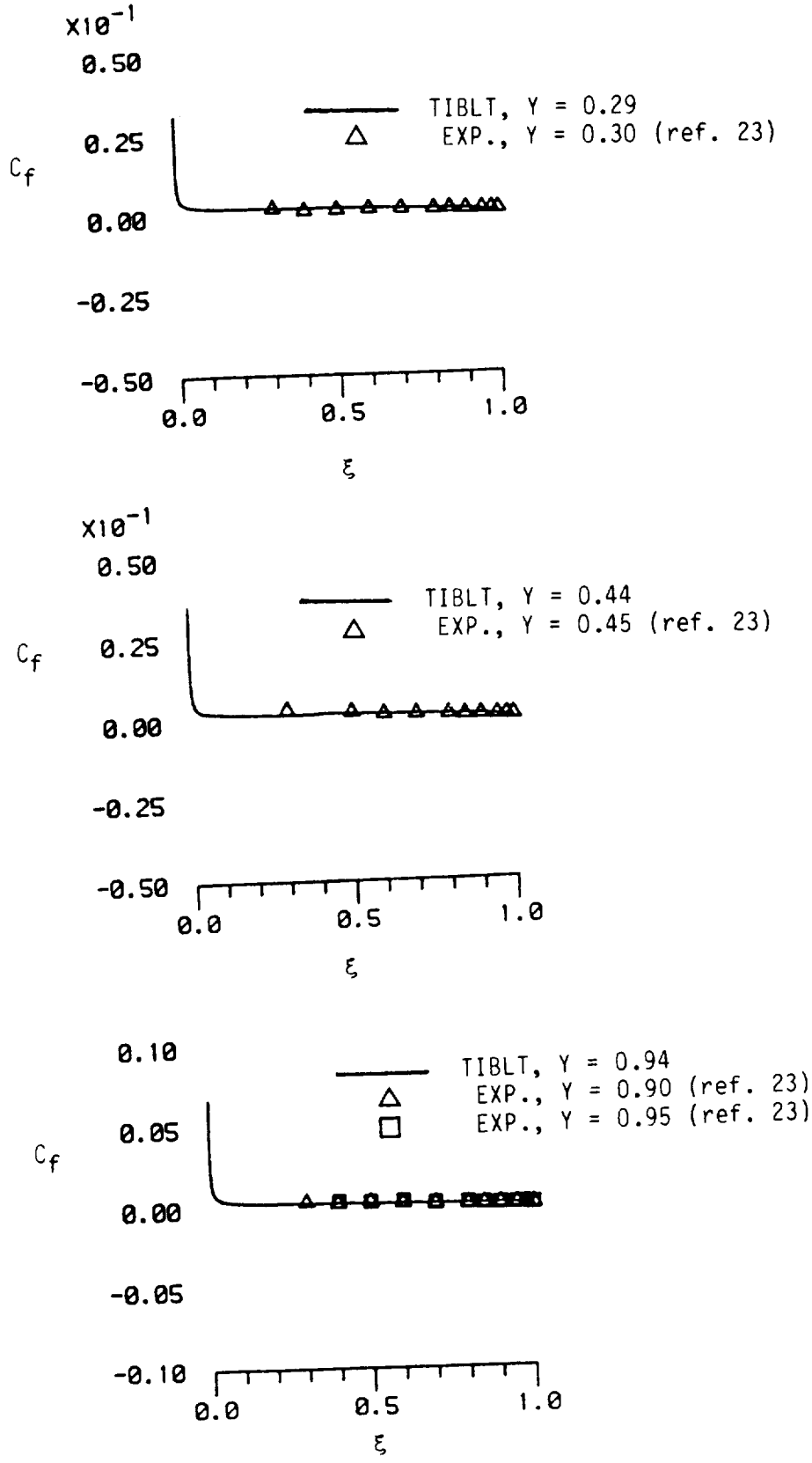

Figure 22. Skin-friction coefficient distribution for the DAC wing, $M_\infty = 0.825$.

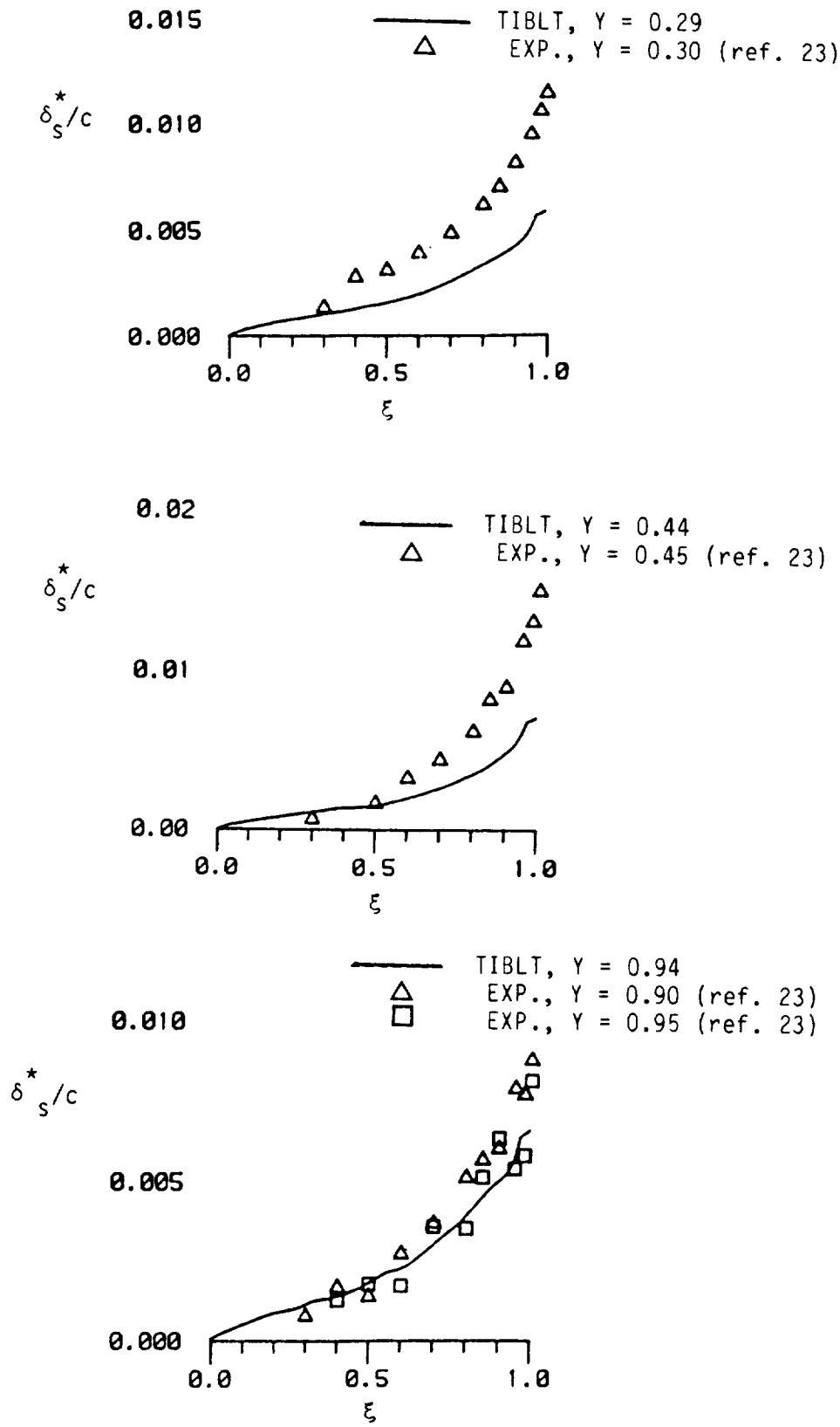

Figure 23. Streamwise velocity integral thickness distribution for the DAC wing, $M_\infty = 0.825$.

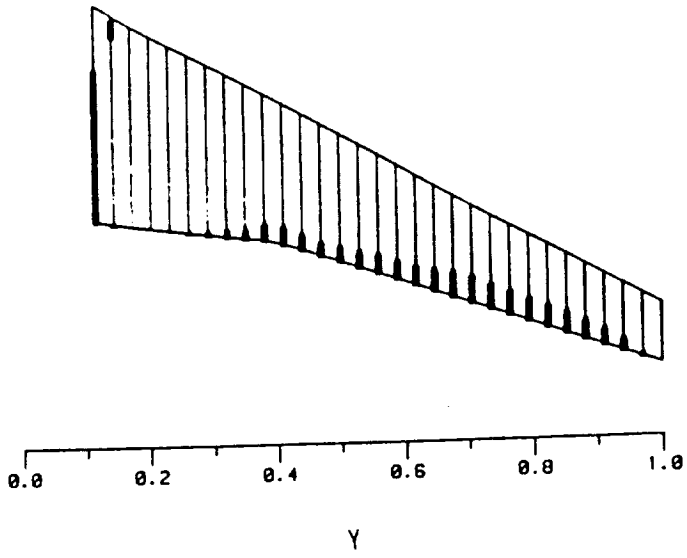

Figure 24. Locations of velocity crossover on the upper surface of the DAC wing, $M_\infty = 0.825$.

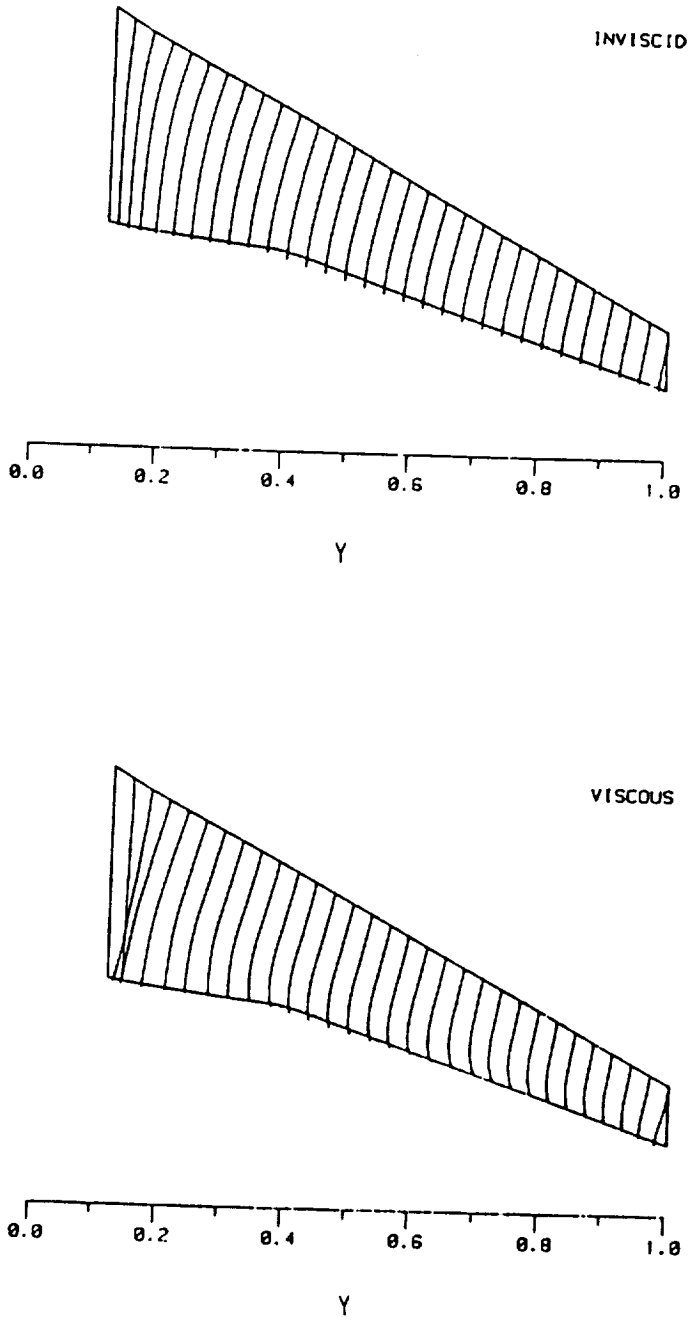

Figure 25.- Inviscid and viscous streamlines for the DAC wing, $M_\infty = 0.825$.

NASA
National Aeronautics and Space Administration

Report Documentation Page

1. Report No.	2. Government Accession No.	3. Recipient's Catalog No.
NASA CR-4185		

4. Title and Subtitle
A Transonic Interactive Boundary-Layer Theory for Laminar and Turbulent Flow Over Swept Wings

5. Report Date
October 1988

6. Performing Organization Code

7. Author(s)
Shawn H. Woodson and Fred R. DeJarnette

8. Performing Organization Report No.

10. Work Unit No.
505-60-21-02

9. Performing Organization Name and Address
North Carolina State University
Department of Mechanical and Aerospace Engineering
Raleigh, NC 23695-7910

11. Contract or Grant No.
NCC1-22

13. Type of Report and Period Covered
Contractor Report

12. Sponsoring Agency Name and Address
National Aeronautics and Space Administration
Langley Research Center
Hampton, VA 23665-5225

14. Sponsoring Agency Code

15. Supplementary Notes
Langley Technical Monitor: James F. Campbell
Final Report

16. Abstract

A three-dimensional laminar and turbulent boundary-layer method is developed for compressible flow over swept wings. The governing equations and curvature terms are derived in detail for a nonorthogonal, curvilinear coordinate system. Reynolds shear-stress terms are modeled by the Cebeci-Smith eddy-viscosity formulation. The governing equations are descritized using the second-order accurate, predictor-corrector finite-difference technique of Matsuno, which has the advantage that the crossflow difference formulas are formed independent of the sign of the crossflow velocity component.

The method is coupled with a full potential wing/body inviscid code (FLO-30) and the inviscid-viscous interaction is performed by updating the original wing surface with the viscous displacement surface calculated by the boundary-layer code. The number of these "global" iterations ranged from five to twelve depending on the Mach number, sweep angle, and angle of attack. Several test cases are computed by this method and the results are compared with another inviscid-viscous interaction method (TAWFIVE) and with experimental data.

17. Key Words (Suggested by Author(s))	18. Distribution Statement
Viscous-inviscid interaction NACA 0012, ONERA M6 Three-dimensional Laminar and turbulent	Unclassified - Unlimited Subject Category 02

19. Security Classif. (of this report)	20. Security Classif. (of this page)	21. No. of pages	22. Price
Unclassified	Unclassified	84	A05

NASA-Langley, 1988

NASA FORM 1626 OCT 86

For sale by the National Technical Information Service, Springfield, Virginia 22161-2171

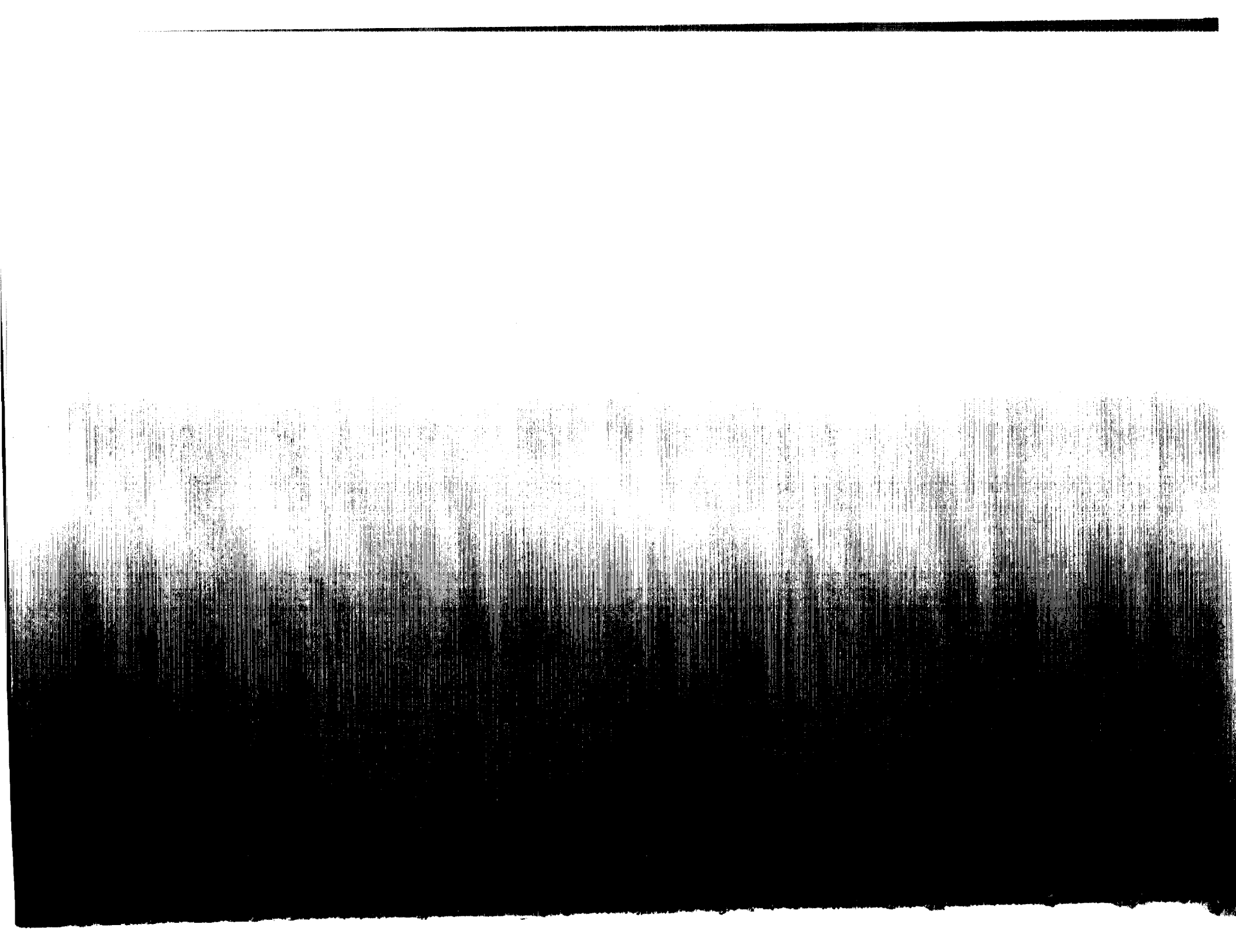

National Aeronautics and
Space Administration
Code NTT-4

Washington, D.C.
20546-0001